

# Europe's Lost Frontiers

General Editor  
Vincent Gaffney

Volume 1

## Context and Methodology

edited by  
Vincent Gaffney and Simon Fitch





# Europe's Lost Frontiers

Volume 1

Context and Methodology

edited by

Vincent Gaffney and Simon Fitch

general editor

Vincent Gaffney



ARCHAEOPRESS PUBLISHING LTD  
Summertown Pavilion  
18-24 Middle Way  
Summertown  
Oxford OX2 7LG

[www.archaeopress.com](http://www.archaeopress.com)

ISBN 978-1-80327-268-9  
ISBN 978-1-80327-269-6 (e-Pdf)

© Archaeopress and the individual authors 2022

Cover: Eleanor Ramsey

This book is available in print and as a free download from [www.archaeopress.com](http://www.archaeopress.com)



This work is licensed under a Creative Commons  
Attribution-NonCommercial-NoDerivatives 4.0 International Licence



Landing by Ava Grauls (Duncan of Jordanstone College of Art & Design).  
Oil and watercolour on Japanese shōji (障子) paper. 413 x 244cm

Landing is about location, ownership, shifting land and shifting borders. The painting was conceived after talking to academics about the space between Britain and Europe, and asking the question: 'How do you paint a forgotten landscape?' Landing was made to travel and interact with different environments and can be folded up and packed away into four boxes.

Ava Grauls 11/08/2021

Dedicated to our Families  
For putting up with Doggerland for longer than any families since the Mesolithic



November 2021

# Europe's Lost Frontiers

**Europe's Lost Frontiers** was funded through a European Research Council Advanced Grant (project number 670518). The European Research Council's mission is to encourage the highest quality research in Europe through competitive funding and to support investigator-driven frontier research across all fields, on the basis of scientific excellence. The European Research Council complements other funding activities in Europe such as those of the national research funding agencies, and is a flagship component of Horizon Europe, the European Union's Research Framework Programme.



**European Research Council**

Established by the European Commission





# Contents

List of Figures .....	iii
General Editor's Preface .....	vii
The Lost Frontiers Team .....	viii
Authors' details .....	ix
Acknowledgements .....	xi
<b>Chapter 1 Europe's Lost Frontiers: context and development.....</b>	<b>1</b>
Vincent Gaffney and Simon Fitch	
<b>Before Europe's Lost Frontiers</b>	
<b>Chapter 2 Beyond the site: A re-evaluation of the value of extensive commercial datasets for palaeolandscape research.....</b>	<b>16</b>
Simon Fitch and Eleanor Ramsey	
<b>Chapter 3 A description of palaeolandscape features in the southern North Sea .....</b>	<b>36</b>
Simon Fitch, Vincent Gaffney, Rachel Harding, James Walker, Richard Bates, Martin Bates and Andrew Fraser	
<b>Chapter 4 From extensive to intensive: Moving into the Mesolithic landscape of Doggerland.....</b>	<b>55</b>
Simon Fitch	
<b>Chapter 5 The archaeological context of Doggerland during the final Palaeolithic and Mesolithic.....</b>	<b>63</b>
James Walker, Vincent Gaffney, Simon Fitch, Rachel Harding, Andrew Fraser, Merle Muru and Martin Tingle	
<b>Europe's Lost Frontiers</b>	
<b>Chapter 6 The Southern River: methods for the investigation of submerged palaeochannel systems .....</b>	<b>89</b>
Simon Fitch, Richard Bates and Rachel Harding	
<b>Chapter 7 Establishing a lithostratigraphic and palaeoenvironmental framework for the investigation of vibracores from the southern North Sea .....</b>	<b>100</b>
Martin Bates, Ben Gearey, Tom Hill, David Smith, John Whittaker and Erin Kavanagh	
<b>Chapter 8 Sedimentary ancient DNA palaeoenvironmental reconstruction in the North Sea landscape.....</b>	<b>112</b>
Robin Allaby, Rebecca Cribdon, Rosie Everett and Roselyn Ware	
<b>Chapter 9 Palaeomagnetic analysis of cores from Europe's Lost Frontiers.....</b>	<b>122</b>
Samuel E. Harris, Catherine M. Batt and Elizabeth Topping	
<b>Chapter 10 Applying chemostratigraphic techniques to shallow bore holes: Lessons and case studies from Europe's Lost Frontiers. ....</b>	<b>137</b>
Alexander Finlay, Richard Bates, Mohammed Bensharada and Sarah Davies	
<b>Chapter 11 Introduction to geochemical studies within Europe's Lost Frontiers .....</b>	<b>154</b>
Mohammed Bensharada, Ben Stern and Richard Telford	

<b>Chapter 12 Constructing sediment chronologies for Doggerland</b> .....	165
Tim Kinnaird, Martin Bates, Rebecca Bateman and Aayush Srivastava	
<b>Chapter 13 Building chronologies for Europe’s Lost Frontiers: Radiocarbon dating and age-depth modelling</b> .....	181
Derek Hamilton and Tim Kinnaird	
<b>Chapter 14 Simulating a drowned landscape: A four-dimensional approach to solving problems of behaviour and scale</b> .....	190
Phil Murgatroyd, Eugene Ch’ng, Tabitha Kabora and Micheál Butler	
<b>Chapter 15 Greetings from Doggerland? Future challenges for the targeted prospection of the southern North Sea palaeolandscape</b> .....	208
Simon Fitch, Vince Gaffney, James Walker, Rachel Harding and Martin Tingle	
 <b>Supplementary Data</b>	
<b>Chapter 16 Supplementary data to ‘The archaeological context of Doggerland during the Final Palaeolithic and Mesolithic’ by Walker, Gaffney, Fitch, Harding, Fraser, Muru and Tingle</b> .....	217
James Walker, Vincent Gaffney, Simon Fitch, Rachel Harding, Andrew Fraser, Merle Muru and Martin Tingle	
<b>Chapter 17 Supplementary data to ‘Constructing sediment chronologies for Doggerbank, North Sea’ by Kinnaird, Bates, Bateman and Srivastava</b> .....	218
Tim Kinnaird, Martin Bates, Rebecca Bateman and Aayush Srivastava	
<b>Bibliography</b> .....	222

# List of Figures

Frontispiece	Landing by Ava Grauls (Duncan of Jordanstone College of Art & Design)	
Figure 1.1	Survey areas prior to Europe’s Lost Frontiers discussed in this chapter. (1) North Sea Palaeolandscape Project (2) Humber REC (3-4) West Coast Palaeolandscape Project. ASTER DEM is a product of METI and NASA. ETOPO2v2 is the property of the National Geophysical Data Centre, NOAA, US Dept of Commerce.....	2
Figure 1.2	Area of Doggerland mapped by the North Sea Palaeolandscape Project (Gaffney <i>et al.</i> 2009: Figure 3.23). .....	3
Figure 1.3	Red flag mapping from Gaffney <i>et al.</i> (2007: Figure 9.8). This image combines threat and uncertainty data based on distance to feature and depth of overlying sediment. The lack of sediment cover and direct association with identified features with archaeological potential rate as high threats with little uncertainty. Deep overlying deposits lying farther from recorded features rank as low threat areas but with significant levels of uncertainty.....	4
Figure 1.4	Distribution of features located within the southern North Sea during the NSPP and BSSS projects.....	6
Figure 1.5	Map used in the final ERC application showing course of two submerged river valleys to be targeted for coring by the Lost Frontiers project team, overlaid on NSPP project base map (Gaffney <i>et al.</i> 2007). .....	8
Figure 1.6	Initial modification of the Europe’s Lost Frontiers coring programme following funding in 2016.....	10
Figure 1.7	Additional modifications to Europe’s Lost Frontiers coring programme following BREXIT.....	11
Figure 1.8	Final Europe’s Lost Frontiers coring programme.....	13
Figure 1.9	Europe’s Lost Frontiers core study area (1), Cardigan and Liverpool Bays (3) and area of study added as part of the Brown Bank survey (2). .....	14
Figure 1.10	Iterative research methodology within Europe’s Lost Frontiers. ....	15
Figure 2.1	Timeslice at 0.076s through the Southern North Sea MegaSurvey 3D seismic dataset. The NSPP study area is outlined in blue and the extended study area discussed within this paper is outlined in red.....	17
Figure 2.2	Graph of the frequency from the PGS MegaSurvey 3D seismic data.....	18
Figure 2.3	Additional, original 3D datasets utilised for comparison with data generated through MegaSurvey processing....	19
Figure 2.4	Data comparison for survey Z3NAM1988A.....	20
Figure 2.5	Frequency values within the 3D legacy seismic volumes assessed within this study.....	21
Figure 2.6	Frequency values within the Parametric Echo Sounder dataset. ....	22
Figure 2.7	Cross-checking between horizontal and vertical slices within the 3D dataset. (A) shows correlation across a wide area with multiple responses along highlighted line, whilst (B) shows the correlation across highlighted line for a single feature.....	4
Figure 2.8	Features within sample area, digitised within SMT Kingdom.....	25
Figure 2.9	Features identified within sample area, imported into an ArcGIS project.....	26
Figure 2.10	Features within the ArcGIS project cleaned and simplified. ....	26
Figure 2.11	A timeslice with opacity filters applied (B), whilst (A) is the resulting interpretation of features derived from image B. It is clear the combination of opacity filters on the timeslice supports fine resolution imaging of small-scale features within this river drainage. ....	27
Figure 2.12	An RMS slice from the Outer Silver Pit area. The slice is generated from the volume between 0s and 0.1s. ....	29
Figure 2.13	Base horizon layer imported from SMT Kingdom into GIS.....	30
Figure 2.14	Areas used to split the horizon point dataset. ....	30
Figure 2.15	Detail within Area 1, showing band divisions used to de-stripe the data. ....	31
Figure 2.16	Interpolated raster of Area 1 prior to manual de-stripping.....	31
Figure 2.17	Interpolated raster of Area 1 after manual de-stripping.....	32
Figure 2.18	3D vertical exaggeration of features within Area 1 using ArcScene. ....	32
Figure 2.19	Interpolated raster mosaic after values for Area 1 and Area 2 had been re-evaluated.....	33
Figure 2.20	A 3D Geobody Model, constructed from the seismic timeslices, and displayed within the seismic volume.....	34
Figure 2.21	A channel visualised by cutting the geobody model to reveal the base of the channel model. By using such methods, it is possible to understand, more fully, the morphology and formation of such structures.....	34
Figure 3.1	GIS Mapping of the features recorded by the Europe’s Lost Frontiers project. ....	37
Figure 3.2	Seismic line from ‘Gauss 159B’ survey acquired in 1990 by the RGD and BGS over the Dogger Bank. A Holocene channel can clearly be seen to be incised into the underlying late Pleistocene deposits (Dogger Bank Formation). .....	37
Figure 3.3	Areas divisions of landscape features within the study area. ....	38
Figure 3.4	Cross section across the southern flank of the Dogger Bank. The Holocene features can be seen to incise into the underlying late Pleistocene deposits.....	39
Figure 3.5	Example of the later Holocene reuse of pro-glacial channels. This is evidenced by smaller (black) channels cut within the main valley and the formation of dendritic feeders on the side of the valley. ....	40
Figure 3.6	The main drainage channels of the Dogger Bank drain south into a major channel located at the foot of the bank and in the area of the Oyster Ground, eventually flowing to the west and into the Outer Silver Pit. ....	41
Figure 3.7	Mottling of the seismic data within the Oyster ground can clearly be seen in this image. A number of small palaeochannels can also be seen through the mottling.....	42
Figure 3.8	Area 1, early Holocene features of the Dogger Bank. The main watersheds are shown as dashed black lines, the features in the southwest of Area 1, including the Shotton River, would have been the longest-lived structures on the Dogger Bank.....	43

Figure 3.9	Map of the Eastern Sector/Area 2.....	44
Figure 3.10	The extent of wetland response is outlined within the red hashed area. The location of BRITICE core 147VC is marked in orange.....	45
Figure 3.11	Interpretation of a seismic line crossing the base of the Dogger Bank area (near the area marked B in Figure 3.8) clearly shows a large channel running at the base of Dogger Bank (shown here as the DB5 unit between 141VC and 140VC) (Roberts <i>et al.</i> 2018: Figure 6).....	46
Figure 3.12	Cross section across the east of the Oyster ground. The topographic rise which forms the watershed is apparent.....	47
Figure 3.13	Location of mapped features within Area 3. ....	48
Figure 3.14	Topographic depressions southeast of the Outer Silver Pit (Area 3).....	49
Figure 3.15	Early Holocene landscape features in Area 4. ....	50
Figure 3.16	Mapped palaeochannels in Area 2 flow towards the -40m bathymetric contour, below this line virtually no features are mapped. This supports the hypothesis that the axial area was a marine inlet during the Holocene/Mesolithic.....	51
Figure 3.17	Major features, Late Palaeolithic c. 11,500 BP. ....	52
Figure 3.18	Coastlines of early Mesolithic Doggerland c. 10,000 BP.....	53
Figure 3.19	Coastlines of Mesolithic Doggerland c. 8500 BP.....	53
Figure 3.20	Coastlines of the earliest Neolithic c. 7000 BP.....	54
Figure 4.1	Location of the Arch-Area_1 study area is shown by a red box. Bathymetric data courtesy of EMODNET Bathymetry Portal, ETOPO1 topographic data courtesy of the NCEI and NOAA.....	56
Figure 4.2	The NSPP 2007 interpretation of the channel system overlain on EMODNET bathymetry.....	57
Figure 4.3	Multibeam Bathymetric image of the survey area generated through the Humber REC.....	58
Figure 4.4	Humber REC 2D seismic line over main channel and tributary channel.....	60
Figure 4.5	Humber REC 2D seismic line showing several strong reflectors in the main channel.....	60
Figure 4.6	A timeslice from the 3D seismic data at 0.076s derived from the PGS Megamerge dataset. The red box is the position of the Humber REC 2D survey, and the position of vibracores VC39/39A and VC40 are shown as yellow circles. ....	61
Figure 4.7	Comparison between the GIS channel outlines as derived from A) the Humber REC 2D survey interpretation and B) the NSPP survey GIS interpretation. Both are overlain on a depth surface derived from the Humber REC 2D dataset.....	61
Figure 5.1	A) The Colinda ‘harpoon’, found within a chunk of ‘moorlog’ peat dredged from the Leman / Ower banks off the Norfolk coast in 1931 (after Flemming 2002); B) A bone point recovered from beach walking at Massvlakte 2 in the Netherlands (courtesy of Luc Amkreutz); C) An array of barbed bone points from Maasvlakte 1 off the Dutch coast (courtesy of the Rijksmuseum van Oudheden). Many other examples of organic artefacts from Dutch waters may be found in Peeters and Amkreutz (2020), Amkreutz and Spithoven (2019) and Louwe Kooijmans (1970).....	65
Figure 5.2	Temperature curve for the Final Pleistocene and Early Holocene (Late Glacial and Postglacial between 17 and 7 thousand years ago) as derived from Greenland Ice Core data, and redrawn from Price (2015). Note the climatic variability of the Final Pleistocene relative to that of the Holocene. ....	66
Figure 5.3	Map showing the projected coastlines of Doggerland and the southern North Sea since the final millennia of the Last Glacial Maximum, with key dates for the transgression highlighted. ....	68
Figure 5.4	The sites and findspots located on the map are a combination of the SplashCOS viewer database, and data points presented in Tables (5.1 and 5.2), with the exception of findspots from Norwegian waters beyond the extent of the map. See this volume, chapter 16 for further information.....	71
Figure 5.5	Four snapshots of landscape evolution across the period of 10,000–7000 cal BP. The period in question spans both the 8.2 ka cold event, and the Storegga tsunami, and shows different stages of Doggerland as it transitioned into an archipelago and, eventually, a littoral fringe landscape.....	76
Figure 5.6	Anders Fischer’s model for the predictive location of submerged Mesolithic sites has been used to great effect in the nearshore waters in and around Denmark. Image from Fischer (2007). The model shows potentially favourable site locations in different coastal landscapes: A) near an estuary mouth or inlet with access to a hinterland; B) in close proximity to islands, but with preference for landward situation; C) on headlands, with particular preference for (D) those offering access to sheltered waters; and E) at river mouths, with preference for (F) flat and even ground.....	78
Figure 5.7	River Valleys active in the Mesolithic, identified through seismic survey and palaeobathymetry, and marked by blue arrows.....	80
Figure 5.8	The location of Core ELF001A where evidence of Storegga tsunami run-up deposits in highly localised areas prompted reconsideration of the event’s impact.....	86
Figure 6.1	The location of the Southern River is within the box on the main map. ....	91
Figure 6.2	The location of the 2D seismic data shown in Figures 6.3 and 6.4 is indicated by the black line (top). The lower image is an example of the original 2D Boomer dataset used for targeting the cores within the Southern River. ..	92
Figure 6.3	2D Boomer data after bandpass filtering applied.....	93
Figure 6.4	2D Boomer data after amplitude and gain correction applied.....	93
Figure 6.5	A combined Bathymetric and seismic data surface of the Southern River. The dendritic network is visible at the head of the river, whilst sinuosity increases as the river proceeds south towards the location of the Holocene coastline. ....	96
Figure 6.6	A seismic cross section showing the position of the Humber REC core Arch VC51 and Europe’s Lost Frontier’s cores ELF006 and ELF001A.....	97
Figure 6.7	The distinctive laminated sediments (SRF6) that produce a clear signal in the seismic data are visible in these images of cores ELF033 and ELF054.....	98

Figure 7.1	Distribution of cores taken during Europe's Lost Frontiers .....	100
Figure 7.2	Flow diagram illustrating pathways of samples in the laboratory. ....	102
Figure 7.3	Cold storage facility for the Lost Frontiers Project at Lampeter (Left). Core recording (Right).....	103
Figure 7.4	Cores ELF 47 and ELF 51.....	105
Figure 7.5	Basic lithological profiles drawn up in the Southern Valley.....	106
Figure 8.1	Differential sedaDNA fragmentation (top) and deamination (bottom) damage patterns in Doggerland palaeoenvironments. Fragmentation expressed as the lambda parameter of the exponential distribution of sedaDNA fragment sizes. Deamination expressed as the probability of observing a C to T change at the terminal position (position 0) of the 5' end of DNA fragments, caused by cytosine deamination.....	115
Figure 8.2	Coring sites used for sedaDNA analysis. A) Cores 1-20. B) Cores in range 21-60 over the Southern River area. C) Cores 20-60. D) Core sites selected for deep sequencing. Estimated 8200 BP coastline shown in black and estimated Storegga tsunami run up extent shown in white. The Storegga tsunami core (ELF001A) shown in grey. ....	120
Figure 9.1	Locations of cores used in this study. ....	122
Figure 9.2	Schematic representation of the detrital remanent magnetisation mechanism from left to right - how the acquisition of the geomagnetic field occurs in sediments. ....	123
Figure 9.3	Location of the UK archaeomagnetic PSVC (Meriden: 52.43°N, -1.62°E), UK Lake Windemere sequence WINPSV_12k (Avery <i>et al.</i> 2017), and FENNOSTACK comprised of seven lake sediment sequences from four lakes (Snowball <i>et al.</i> 2007). ....	124
Figure 9.4	Sampling of core ELF019 during the first sampling trip (© Erin Kavanagh).....	125
Figure 9.5	Palaeomagnetic analysis procedure followed when full analysis takes place. ....	127
Figure 9.6	Comparison of the Inclination data isolated through PCA with associated errors against the WINPSV-12k (Avery <i>et al.</i> 2017) calibration curve. ....	128
Figure 9.7	Left: Magnetic susceptibility values for core ELF001A averaged from three separate runs and corrected for drift of sensor. Features on the plot are noted in the text. Right: Image of the core for comparisons. ....	129
Figure 9.8	Stratigraphic trends of the rock magnetic parameters for ELF001A. The plots show the variations in a) magnetic susceptibility, b) susceptibility of ARM, c) S-ratio, d) Saturation Isothermal Remanent Magnetisation (SIRM), e) ARM <sub>x</sub> /SIRM ratio, f) percentage of bIRM acquired between 0-20mT, and g) the Coercivity of Remanence.....	131
Figure 9.9	Left: Magnetic susceptibility values for core ELF002 averaged from three separate runs and corrected for drift sensor. Features on the plot are noted in the text. Right: Image of the core for comparisons.....	132
Figure 9.10	Left: Magnetic susceptibility values for core ELF003 averaged from three separate runs and corrected for drift sensor. Features on the plot are noted in the text. Right: Image of the core for comparisons.....	133
Figure 9.11	Left: Magnetic susceptibility values for core ELF019 averaged from three separate runs and corrected for drift sensor. Features on the plot are noted in the text. Right: Image of the core for comparisons.....	134
Figure 9.12	The declination and inclination values plotted down core for ELF019 from the analysis of 21 samples.....	135
Figure 9.13	Down core plot of magnetic proxies calculated for core ELF019. ....	135
Figure 10.1	A summary of the benefits of typical analytical tools utilised in chemostratigraphic studies and their acronyms.....	138
Figure 10.2	Location map of cores referred to in this paper. Bathymetric data is derived from the EMODnet Bathymetry portal - <a href="http://www.emodnet-bathymetry.eu">http://www.emodnet-bathymetry.eu</a> . Topographic data derived from the NOAA ETOPO1 dataset, courtesy of the NCEI - <a href="https://www.ngdc.noaa.gov/mgg/global/">https://www.ngdc.noaa.gov/mgg/global/</a> .....	140
Figure 10.3	PCA of elemental data for core ELF19 showing the likely mineralogical and material drivers for variation in elemental compositions. a - component 1 and 2, b - component 2 and 3.....	141
Figure 10.4	Chemostratigraphic zonation of core ELF19. Si/Rb likely reflects variations in grain size with higher values being more Sand (Quartz) rich and higher Rb being more Clay rich. Ca/Rb likely reflects variations in carbonate (Ca) compared to clay material. S/Rb likely reflects variations in organic material (S) to clay. Br/Ti is a proxy for salinity in wetlands (see text for references).....	142
Figure 10.5	Boxplots showing the correlation of observed mineralogy and chemistry within core ELF19. ....	144
Figure 10.6	This figure demonstrates an excellent match in the chemostratigraphic zonation of core ELF19 and ecological biostratigraphic data.....	146
Figure 10.7	Orkney core locations .....	147
Figure 10.8	The elemental variations utilised to define the chemostratigraphic zonation in the study area. Sr/Br likely reflects variations in shell material (Sr - aragonite) and organic material (Br). Sr/Rb likely reflects variations in shell material (Sr - aragonite) and Clay (Rb). Si/Br likely reflects variations in sand (Si - Quartz) and organic material (Br). ....	148
Figure 10.9	Chemostratigraphic correlation of chemo zones in wells A, B and C.....	149
Figure 10.10	Chemostratigraphic correlation of chemo sub zones in wells A, B and C. ....	149
Figure 10.11	Chemostratigraphic zonation of core ELF1A (from Gaffney <i>et al.</i> 2020). Sr likely reflects the amount of shell material (aragonite) Rb likely reflects the amount of clay, Si likely reflects the amount of sand (Quartz) and Zr the amount of detrital zircon in the core. ....	150
Figure 10.12	Chemostratigraphic zonation of the Storegga tsunami deposit preserved in core ELF1A (from Gaffney <i>et al.</i> 2020).....	150
Figure 10.13	Comparison of the relative density of core ELF1A calculated from XRF data to the interpreted seismic data (from Gaffney <i>et al.</i> 2020). ....	152
Figure 11.1	Locations of the three cores mentioned in the text.....	155
Figure 11.2	Extracted ion chromatogram (EIC), for 71m/z showing n-alkanes in the sample ELF002. ....	157
Figure 11.3	Extracted ion chromatogram (EIC) for 71m/z, showing n-alkanes in the sample ELF007 .....	157

Figure 11.4	Extracted ion chromatogram (EIC) for 71m/z, showing n-alkanes in the sample ELF009. ....	157
Figure 11.5	Fatty acids found in sample ELF002. ....	159
Figure 11.6	Fatty acids found in sample ELF007. ....	159
Figure 11.7	Fatty acids found in sample ELF009. ....	159
Figure 11.8	XRD pattern of sample ELF002. ....	160
Figure 11.9	XRD pattern of sample ELF007. ....	160
Figure 11.10	XRD pattern of sample ELF009. ....	160
Figure 11.11	Comparison between the ELF002 pattern and the standard of quartz, berlinite and calcite. ....	162
Figure 11.12	PXRD of ELF007 overlain with reference patterns of quartz, berlinite and halite. ....	163
Figure 11.13	PXRD of ELF009 overlain with reference patterns of quartz and halite. ....	163
Figure 12.1	Locations of cores mentioned in text. ....	166
Figure 12.2	For successful OSL dating, both environmental and mineral characteristics are important: zeroing during transport and deposition is a function of environmental conditions and luminescence behaviour. ....	167
Figure 12.3	Illustrative luminescence-depth plots for the Doggerland cores: illustrating, (A., ELF05B) stratigraphic breaks and temporal discontinuities, (B., ELF012) rapid sedimentation and short chronology, (C., ELF022) slow sedimentation and long chronology, (D., ELF051) stratigraphic breaks, stratigraphic progressions and cyclicity. ....	169
Figure 12.4	Sampling strategy for ELF cores – illustrated with core ELF001A: (a) core, with sub-units identified; (b) core, with sampling positions indicated; (c) removal of sediment for OSL profiling, OSL dating and dosimetry. ....	171
Figure 12.5	Illustrative luminescence-depth plots for ELF001A: on the left, IRSL and OSL net signal intensities and depletion indices; on the right, apparent dose and sensitivity distributions. ....	172
Figure 12.6	D <sub>e</sub> distributions for ELF001A, 90-150µm, shown relative to the stratigraphy of the core. Units for ELF001A as discussed in the text. ....	177
Figure 12.7	Stored dose estimates for the 90-150µm and 150-250µm quartz fractions. ....	178
Figure 12.8	Dosimetry of core ELF001A: semi-quantitative and absolute down-core variations in radionuclide concentrations. ....	179
Figure 12.9	(left) Apparent vs stored dose estimates for discrete depths in core across a subset of sampled cores, encompassing terrestrial, littoral and marine deposits; (right) Quartz SAR OSL depositional ages shown relative to depth in core for the same subset of cores. ....	180
Figure 13.1	Locations of cores mentioned in this chapter. ....	183
Figure 13.2	Age-depth model for ELF001A. Each distribution represents the relative probability that an event occurred at some particular time. For each OSL measurement two distributions have been plotted, one in outline, which is the original result, and a solid one, which is based on the chronological model use. The other distributions correspond to aspects of the model. For example, 'start: Unit 5' is the estimated date that this litho-stratigraphic change occurred, based on the dating results. The large square 'brackets' along with the OxCal keywords define the overall model exactly. ....	184
Figure 13.3	Age-depth model for ELF007. The model is described in Figure 13.2, with the exception that the outline of the radiocarbon dates is based on the simple calibration of those measurements, whereas the solid ones are the result of the modelling. ....	186
Figure 13.4	Age-depth model for ELF034. The model is as described in Figures 13.2 and 13.3. ....	187
Figure 13.5	Calibrated humin fraction and humic acid pairs for depths 180, 185, 193, 202, and 209cm in core ELF034. ....	188
Figure 13.6	Detail of the bottom of the age-depth model for ELF034. In this detail the humin fraction and humic acid dates at each level have been plotted side-by-side, rather than combined as in Fig 13.4, to show the relationship of each result to the conservative model results for the bottom of the core. ....	189
Figure 14.1	The simulation conceptual framework. ....	196
Figure 14.2	3D visualisation package, showing part of the Southern River valley terrain with simulated sea level. ....	197
Figure 14.3	A 3D render of the output of the forest dynamic modelling package. ....	198
Figure 14.4	Graphical output from the landscape modelling package showing areas with differing amounts of inundation over time. ....	198
Figure 14.5	A screenshot of the quadtree-based large-scale modelling infrastructure, showing herbivore agents responding to resources in a landscape. The red squares show the dynamic partitioning of the environment resulting from the quadtree structure. ....	199
Figure 14.6	The ELF Augmented Reality sandbox. ....	200
Figure 14.7	The ELF Augmented Reality sandbox in use. ....	200
Figure 14.8	The Model 1.1 simulation study area. ....	201
Figure 14.9	Relative sea-level change over the last 21,000 years in the North Sea region from Glacial Isostatic Adjustment (GIA) model reconstructions (Bradley <i>et al.</i> 2011; Shennan, Bradley and Edwards 2018). ....	203
Figure 14.10	Table of data showing headings. ....	204
Figure 14.11	Graph showing one calendar year's data of water height and atmospheric pressure effect. ....	204
Figure 14.12	Graph showing 14 year's water height data. ....	205
Figure 14.13	Flowchart of the Europe's Lost Frontier models. ....	206
Figure 15.1	Areas designated for windfarm development within UK and Belgian waters and survey lines associated with the Brown Bank and Southern River study areas (The Crown Estate ©, bathymetry derived from EMODNET. Topography derived from ETOPO) ....	209
Figure 15.2	Survey on the Southern River estuary ....	211
Figure 15.3	A flint hammerstone fragment, approximately 50mm wide, was retrieved during a 2019 survey of the Southern River valley (offshore north of the Norfolk coast) from (or near) a surface dated to 8827±30 cal BP SUERC-85715 (Missiaen <i>et al.</i> 2021). Scanned image courtesy of Tom Sparrow. ....	213
Figure 17.1	Equivalent dose distributions for units 4, 5, 6 and 7 from ELF001A as histogram plots ....	221

## List of Tables

Table 1.1	Numbers and area of features, excluding coastlines, identified through the NSPP and BSSS projects (2008-2012). After Gaffney <i>et al.</i> 2011: Table 5.1 .....	7
Table 2.1	Additional, original 3D datasets used for cross comparison purposes. ....	19
Table 5.1	Mesolithic sites and findspots from territorial waters, the nearshore zone (<12 nautical miles of the shoreline) of the North Sea basin. This table excludes submerged sites and findspots located from inland waters (rivers, inlets and estuaries) in Essex (UK) and the Limfjord (Denmark). For category Type: CF = Collection of Finds; SF = Single Find; (U) = Unstratified; (S) = Stratified. For category Dating: C14 = Radiocarbon Dating; T-C = Typo-chronology; Strat = Stratigraphically; SLC = Sea Level Curve. For Sources, BMAPA stands for British Marine Aggregate Producers Association. Age estimates are given in approximate years BC, and depth is given in metres. Some locales comprise multiple findspots, and grid references are approximate. Data primarily compiled using SplashCOS Viewer available at <a href="http://www.SplashCOS.maris2.nl">www.SplashCOS.maris2.nl</a> .....	70
Table 5.2	Palaeolithic, Mesolithic and Neolithic findspots from the offshore zone beyond territorial waters (>12 nautical miles of the shoreline) of the North Sea basin. For category Type: CF = Collection of Finds; SF = Single Find; (U) = Unstratified; (S) = Stratified. For category Dating: C14 = Radiocarbon Dating; T-C = Typo-chronology; Strat = Stratigraphically. For category Sources: RMO stands for Rijksmuseum van Oudheden. Age estimates are given in approximate years BC, and depth is given in metres. Some locales comprise multiple findspots, and grid references are approximate. Data primarily compiled (excluding the Southern River find) using SplashCOS Viewer available at <a href="http://www.SplashCOS.maris2.nl">www.SplashCOS.maris2.nl</a> .....	70
Table 6.1	Geological deposits within the study area.....	90
Table 6.2	Seismic facies within the Southern River system .....	99
Table 7.1	ELF 045, lithology table.....	104
Table 7.2	Cores sampled in project. Abbreviations as follows: P1, profile 1, uncalibrated OSL; P2, profile 2, calibrated OSL; D, OSL sediment ages.....	108
Table 7.3	Example of data from rapid assessment of cores samples.....	109
Table 7.4	Detailed assessment of microfossils from ELF 047. ....	110
Table 7.5	Cores selected for pollen and diatom investigation. ....	111
Table 7.6	Cores samples for macrofossil analysis.....	111
Table 9.1	Summary of palaeomagnetic sampling details with core locations.....	126
Table 9.2	The stage of palaeomagnetic analysis carried out on each core to date: X denotes completion, P denotes partial analysis. Magnetic susceptibility carried out on obtained samples at the University of Bradford (1) and carried out using the handheld MS2K directly on the core sections (2).....	127
Table 9.3	Definitions of magnetic proxies referred to in text and used to characterise the magnetic minerals present.....	130
Table 10.1	Elements commonly utilised for archaeological and paleoenvironmental research (summarised from Davies <i>et al.</i> 2015 and Chemostrat multiclient report NE118).....	139
Table 10.2	Likely elemental affinities for core ELF19. ....	142
Table 10.3	Chemical definition of Chemo Zones and boundaries for core ELF19. ....	143
Table 10.4	Integrated chemical and ecological results for core ELF19. ....	145
Table 10.5	Chemical, sedimentological and environmental interpretation of chemo zones and integrated facies identification.....	148
Table 10.6	Chemo facies identified in core ELF1A (see Gaffney <i>et al.</i> 2020 supplementary information for full discussion). ..	151
Table 10.7	A summary interpretation of geochemical and seismic datasets.....	153
Table 11.1	Core identifiers, location and depth.....	155
Table 11.2	The percentage of organics and carbonates. ....	156
Table 11.3	Characteristic (2 $\theta$ ) values, and the d-spaces of standards and the obtained samples pattern. ....	161
Table 12.1	Stored dose estimates for the 90-150 $\mu$ m quartz fractions from ELF001A (lab code, CERSA114). ....	178
Table 12.2	Weighted combinations of OSL depositional ages for ELF001A. ....	179
Table 17.1	Observations / inferences from preliminary OSL screening and subsequent calibrated OSL characterisation, example ELF001A.....	219

# The Lost Frontiers Team

## **University of Bradford**

Dr Andrew Fraser  
Dr Ben Stern  
Dr Catherine Batt  
Dr James Walker  
Dr Philip Murgatroyd  
Dr Rachel Harding  
Dr Richard Telford  
Dr Simon Fitch  
Dr Tabitha Kabora  
Micheál Butler  
Mohammed Bensharada  
Professor Vincent Gaffney  
Sam Harris  
Dr Helen McCrearey  
Elizabeth Topping  
Anne Harvey  
Tim Squire-Watt

## **University of Aberystwyth**

Professor Sarah Davies

## **University of Bath**

Dr Matt Law

## **University of Birmingham**

Dr David Smith  
Eamonn Baldwin

## **Chemostrat**

Dr Alexander Finlay

## **University College Cork**

Dr Ben Gearey  
Dr Kevin Kearney

## **Flanders Marine Institute**

Dr Tine Missiaen  
Dr Ruth Plets

## **National University of Ireland, Galway**

Eoghan Daly

## **University of Glasgow**

Dr Derek Hamilton

## **INFOMAR**

Kevin Sheehan

## **Natural History Museum**

Dr John Whittaker

## **University of Nottingham, Ningbo**

Professor Eugene Ch'ng

## **PalaeoEnvironmental Research and Consultancy Services Ltd**

Dr Tom Hill

## **Sligo Institute of Technology**

Dr James Bonsall  
Eithne Davis

## **University of Wales, Trinity St Davids**

Dr Martin Bates  
Erin Kavanagh

## **University of St Andrews**

Professor Richard Bates  
Dr Tim Kinnaird  
Rebecca Bateman  
Aayush Srivastava

## **University of Tartu**

Dr Merle Muru  
Dr Alar Rosentau

## **University of Warwick**

Dr Rebecca Cribdon  
Dr Roselyn Ware  
Professor Robin Allaby  
Dr Rosie Everett

## **Wolverhampton and Walsall Historic Environment Record**

Eleanor Ramsey

Dr Martin Tingle  
Dr Wendy Carruthers



## Authors' details

Robin Allaby, School of Life Sciences, Gibbet Hill Campus, University of Warwick, Coventry CV4 7AL, United Kingdom

Rebecca Bateman, School of Earth and Environmental Sciences, University of St Andrews, Bute Building, Queen's Terrace, St Andrews KY16 9TS, United Kingdom

Martin Bates, Faculty of Humanities and Performing Arts, University of Wales Trinity Saint David, Lampeter, Ceredigion SA48 7ED, United Kingdom

Richard Bates, School of Earth and Environmental Sciences, University of St Andrews, Bute Building, Queen's Terrace, St Andrews KY16 9TS, United Kingdom

Catherine M. Batt, School of Archaeological and Forensic Sciences, University of Bradford, Richmond Road, Bradford BD7 1DP, United Kingdom

Mohammed Bensharada, School of Archaeological and Forensic Sciences, University of Bradford, Richmond Road, Bradford BD7 1DP, United Kingdom

Micheál Butler, School of Archaeological and Forensic Sciences, University of Bradford, Richmond Road, Bradford BD7 1DP, United Kingdom

Eugene Ch'ng, NVIDIA Technology Centre, University of Nottingham Ningbo China, 199 Taikang East Road, Ningbo 315100, China

Rebecca Cribdon, School of Life Sciences, Gibbet Hill Campus, University of Warwick, Coventry CV4 7AL, United Kingdom

Sarah Davies, School of Geography and Earth Sciences, Llandinam Building, Penglais Campus, Aberystwyth University, Aberystwyth SY23 3DB, United Kingdom.

Rosie Everett, School of Life Sciences, Gibbet Hill Campus, University of Warwick, Coventry CV4 7AL, United Kingdom

Alexander Finlay, Chemostrat Ltd., 1 Ravenscroft Court, Buttington Cross Enterprise Park, Welshpool, Powys SY21 8SL, United Kingdom

Simon Fitch, School of Archaeological and Forensic Sciences, University of Bradford, Richmond Road, Bradford BD7 1DP, United Kingdom

Andrew Fraser, School of Archaeological and Forensic Sciences, University of Bradford, Richmond Road, Bradford BD7 1DP, United Kingdom

Vincent Gaffney, School of Archaeological and Forensic Sciences, University of Bradford, Richmond Road, Bradford BD7 1DP, United Kingdom

Ben Gearey, Department of Archaeology, Connolly Building, Dyke Parade, University College, Cork, Cork City T12 CY82, Ireland

Derek Hamilton, Scottish Universities Environmental Research Centre, Rankine Avenue, Scottish Enterprise Technology Park, East Kilbride G75 0QF, United Kingdom

Rachel Harding, School of Archaeological and Forensic Sciences, University of Bradford, Richmond Road, Bradford BD7 1DP, United Kingdom

Samuel E. Harris, School of Archaeological and Forensic Sciences, University of Bradford, Richmond Road, Bradford BD7 1DP, United Kingdom

Tom Hill, PalaeoEnvironmental Research and Consultancy Service, 67 Eastfield Road, Princes Risborough, Buckinghamshire HP27 0HZ / Department of Earth Sciences, The Natural History Museum, Cromwell Road, London SW7 5BD, United Kingdom.

Tabitha Kabora, Leverhulme Centre for Anthropocene Biodiversity, University of York, York YO10 5DD, United Kingdom

Erin Kavanagh, Arts Building, University of Birmingham, Edgbaston, Birmingham B15 2TT, United Kingdom

Tim Kinnaird, School of Earth and Environmental Sciences, University of St Andrews, Bute Building, Queen's Terrace, St Andrews KY16 9TS UK

Philip Murgatroyd, School of Archaeological and Forensic Sciences, University of Bradford, Richmond Road, Bradford BD7 1DP, United Kingdom

Merle Muru, Department of Geography, University of Tartu, 46 Vanemuise Str, 51003 Tartu, Estonia

Eleanor Ramsey, Wolverhampton and Walsall Historic Environment Record, Wolverhampton City Council, Civic Centre, St Peter's Square, Wolverhampton, WV1 1RP, United Kingdom.

David Smith, Classics, ancient History and Archaeology,  
University of Birmingham, Edgbaston, Birmingham B15  
2TT, United Kingdom

Aayush Srivastava, School of Earth and Environmental  
Sciences, University of St Andrews, Bute Building,  
Queen's Terrace, St Andrew, KY16 9TS, United Kingdom.

Ben Stern, School of Archaeological and Forensic  
Sciences, University of Bradford, Richmond Road,  
Bradford BD7 1DP, United Kingdom

Richard Telford, Centre for Chemical and Biological  
Analysis, University of Bradford, Richmond Road,  
Bradford BD7 1DP, United Kingdom

Martin Tingle, 106 Brook Street, Wymeswold LE12 6TU,  
United Kingdom

Elizabeth Topping, School of Archaeological and  
Forensic Sciences, University of Bradford, Richmond  
Road, Bradford BD7 1DP, United Kingdom

James Walker [Archaeological Museum](#), University of  
Stavanger, 4036 Stavanger, P.O. box 8600, Norway

Roselyn Ware, School of Life Sciences, Gibbet Hill  
Campus, University of Warwick. Coventry CV4 7AL,  
United Kingdom

John Whittaker, Department of Earth Sciences, The  
Natural History Museum, Cromwell Road, London SW7  
5BD, United Kingdom.

## Chapter 10

# Applying chemostratigraphic techniques to shallow bore holes: Lessons and case studies from Europe's lost Frontiers

Alexander Finlay, Richard Bates, Mohammed Bensharada and Sarah Davies

### Introduction

The range of applications of analytical geochemistry in the geosciences extends from hydrocarbon studies to forensic investigations with samples from billion year old material formed deep within the earth to material from contemporary environments (Poulton *et al.* 2010). Within archaeological and palaeoenvironmental research, elementary geochemistry can also provide an excellent analytical tool for the investigator. There are numerous examples of these techniques being applied, from the provenance and identification of manufacture of anthropogenic material (e.g. Finlay *et al.* 2012) through to palaeoenvironmental studies e.g. Croudace and Rothwell (2015). This chapter will demonstrate how geochemical and chemostratigraphic techniques have been applied within the *Europe's Lost Frontiers* project. A review of commonly utilised analytical techniques in archaeological and paleoenvironmental studies is first presented, followed by details on the methods of data collection, quality control and interpretation. Key cores are used as case studies to demonstrate particular aspects of the method.

Case study 1 demonstrates how geochemical analysis can be utilised to characterise a core into a series of chemostratigraphic zones (chemo zones), assign these to geochemical facies (chemo facies) reflecting their depositional environment and then validate these chemo facies by integrating them with other ecological datasets.

Case study 2 demonstrates how a comparison of chemo zones and facies from multiple cores within a study area can be used to produce a regional chemostratigraphic correlation, and so aid palaeolandscape reconstruction.

Case study 3 demonstrates the integration of chemostratigraphy with other methods such as seismic interpretation through the production of chemical modelled density profiles to link to the seismic data. This in turn is utilised for a greater understanding of the spatial coverage of the chemo zones and interpreted facies.

The chapter concludes with an overview of other applications of geochemical analysis that may be applied to future studies using unconsolidated sediment cores and palaeoenvironmental reconstruction.

### Elemental analysis

#### *Quantitative methods*

The range of geochemical analysis techniques available for sediment quantitative elemental data include inductively coupled plasma-optical emission spectrometer (ICP-OES), inductively coupled plasma mass spectrometry (ICP-MS) and X-ray fluorescence (XRF Figure 10.1 e.g. Jarvis and Jarvis 1992; Ratcliffe *et al.* 2012). ICP-MS and ICP-OES are laboratory based elemental tools requiring significant sample preparation including microwave, flux fusion or acid digest processes in order to place the sample into a solution prior to analysis (Olesik 1991). The ICP-MS detects the mass of the ions hitting its detector and provides a mass spectrum for the sample, with the intensity of each mass peak in the spectrum being directly proportional to the concentration of an element of the same mass within the sample. The mass is quantified by comparing the intensities of the mass spectrum to known calibration standards (Tyler and Jobin Yvon 1995). The ICP-OES differs in that it measures the effect of the ions on the sample on the plasma itself. When the sample solution is introduced to the plasma the elements contained within loose electrons and give off radiation with wavelengths characteristic to the element itself. The optical spectrometer detects this radiated energy, and through comparison with the intensities of known calibration standards the elemental abundance can be quantified within the sample (Jarvis and Jarvis 1992; Olesik 1991; Tyler and Jobin Yvon 1995). The combined use of both ICP-MS and ICP-OES enable the quantification of major elements (greater than one weight percent of the sample) and trace elements (typically down to parts per billion level; Jarvis and Jarvis 1992).

X-ray fluorescence (XRF) is the emission of characteristic 'secondary' (or fluorescent) X-rays from a material that has been excited by being bombarded with high-energy X-rays. Analytical tools vary from laboratory-based techniques that can produce analysis similar to ICP instruments to highly portable handheld tools that can be used in the field. Dependant on lithology it provides data for ten major and approximately twenty trace elements, importantly including both chlorine

Laboratory based	Inductively coupled plasma mass spectrometry (ICP-MS)	Inductively Coupled Plasma Optical Emission spectroscopy (ICP-OES)	Wavelength dispersive X-ray fluorescence (WD- XRF)	Energy Dispersive X-ray fluorescence (ED- XRF)	Hand held X-ray fluorescence (HH-XRF)
Field based					
Increasingly lower limits of detection	← - - - - -				
Increasing cost of analysis	← - - - - -				
Increasing speed of analysis	- - - - - →				

Figure 10.1 A summary of the benefits of typical analytical tools utilised in chemostratigraphic studies and their acronyms.

and sulphur making it the ideal tool for analysing saline samples. Handheld X-Ray Fluorescence is capable of providing rapid elemental data (Hennekam and de Lange 2012; Schmidt *et al.* 2018). The tool is non-destructive and capable of high spatial resolution analysis thus making it ideal for use in core scanning (Schmidt *et al.* 2018). However, it does not have the same limits of detection that more powerful x-ray tools possess.

#### Qualitative methods – Scanning/Micro XRF

An ITrax X-Ray Fluorescence core scanner (Cox Analytical Systems), based at Aberystwyth University, was used in *Europe's Lost Frontiers* project. The ITrax is a laboratory XRF scanner capable of very high resolution, continuous environmental core scanning at a relatively rapid automated rate (Croudace and Rothwell 2015). While the data it collects is quantitative there are currently no standard reference materials for the technique and thus results are more appropriate to analysis of relative changes in elemental abundance rather than absolute elemental values reported by techniques such as ICP-MS. In *Europe's Lost Frontiers*, the ITRAX provided data at a resolution of 0.5mm thus allowing for chemical fingerprints of very short-lived climatic, depositional, and environmental changes. An additional benefit of the ITrax is its ability to record the incoherent (Compton) and coherent (Rayleigh) scattering caused by the XRF interaction with the core, enabling key information such as core density to be calculated (e.g. Fortin *et al.* 2013; Gaffney *et al.* 2020). Calculation of core density enables a comparison to be made of the geochemistry with other regional remote sensing techniques such as seismic analysis.

#### Data acquisition, quality control, data processing

A single data quality control and interpretation method was developed and utilised for all cores in the *Europe's Lost Frontiers* project in order to ensure that, as much as possible, data from different cores collected at different times was comparable.

The cores were initially split lengthwise, and the exposed surface scraped to ensure a smooth and flat surface. The scanner was typically set for a resolution of 0.5mm along core-interval and a dwell time of 15 seconds with the x-ray tube at 30kV and 50mA. For the individual core sections, the scanning line was adjusted to avoid sampling holes. All reported data was smoothed using a  $\pm 4$ mm moving average filter applied to the data in order to remove any 'nugget' effect caused by clasts of a specific elemental composition leading to an overestimate of those elements compared to that of the core (e.g. Croudace and Rothwell 2015; Gaffney *et al.* 2020).

To test the validity of the recorded data, distance to sample surface, total counts and Argon (as the Ar signal is derived from the excitation of argon in air between the sample and X-ray source, rather than the sample) was plotted by core depth (below surface) and compared to the ITrax chemical data. A fall in total counts that coincides with a peak in Ar, suggest that any changes in chemical data at these depths may be caused by physical damage or irregularities in the core surface rather than elemental variations in the core (Croudace and Rothwell 2015). If these conditions were met, then the elemental data from these depths was not utilized in this study. Furthermore, any data that were outside two standard deviations of the mean depth to sample

Element	Symbol	Common mineralogical control	Common interpretations
Aluminium	Al	Clays	Depositional energy/Grain size
Bromine	Br	Organic material	Productivity/Salinity/marine influence
Calcium	Ca	Calcite	Evaporite or marine signal
Iron	Fe	Heavy and/or clay minerals	Detrital input
Potassium	K	Clay minerals	Detrital input and depositional energy
Magnesium	Mg	Dolomite	Dolomitisation
Sodium	Na	Halite	Salinity
Phosphorus	P	Apatite and phosphates	Heavy minerals or Nutrient enrichment
Sulphur	S	Organic material/Gypsum	Productivity/Salinity/marine influence/palaeosoils
Silica	Si	Quartz	Depositional energy/Grain size
Strontium	Sr	Aragonite	Shell material/marine signal
Thorium	Th	Heavy minerals	Depositional energy/Grain size. Link with gamma ray logs
Titanium	Ti	Heavy and/or clay minerals	Detrital input
Uranium	U	Heavy minerals or anoxia	Depositional energy/Grain size. Organic content. Link with gamma ray logs
Zirconium	Zr	Heavy minerals	Depositional energy/Grain size

Table 10.1 Elements commonly utilised for archaeological and paleoenvironmental research (summarised from Davies *et al.* 2015 and Chemostrat multiclient report NE118).

surface, thus indicating an irregular surface, were also treated with caution.

Three methods are proposed to ensure confidence in using ITrax derived identification of mineralogical or deposition drivers for variations in elemental chemistry. Where possible, additional quantitative mineralogical analysis (e.g. X-ray Diffractions/Raman mineralogy or SEM-EDS techniques) on a subset of samples can be made for comparison of the sediment chemistry with the mineralogy. If additional data is not available, a comparison with observed changes in the core from more traditional methods such as colour, shell fragments and grain size can be made. Finally, the data can be analysed using statistical methods such as principal component analysis (PCA).

Principal Component Analysis (PCA) is a mature statistical technique that is widely used for identifying patterns in data of multiple dimensions. PCA finds a set of orthogonal dimensions, which account for the variance in a specific dataset, by reducing the dimensionality of a complex system of correlations into a smaller number of dimensions. The first principal component accounts for as much data variance as possible and each subsequent principal component accounts for remaining data variance (Michoux 2020). For example, in a hypothetical interbedded sand/mud section that transitions from marine to fluvial control, PCA1 would likely be controlled by a variation in elements associated with the sand (e.g. Si and Zr) and clay fractions (e.g. Al, Rb and K), whereas PC2 may be marked by the variation between these detrital

minerals and elements associated with marine settings (Ca and Sr).

An in-depth review of possible controls in elemental data are reported by Rothwell and Croudace (2015) for marine sediments and Davies *et al.* (2015) for fluvial sediments. Table 10.1 lists the common drivers of elemental variation within sedimentary units. However, it is stressed that sediments are complex mixtures of natural materials and so this may not always be true.

### ***Case study 1 - Chemostratigraphic zonation, chemostratigraphic facies and integration with sedimentological and ecological data to establish the depositional environment of Core ELF19***

#### *Introduction*

Case study 1 comprises a comparison of elemental data to microfossil analysis and observed variations in mineralogy within core ELF19. This was collected off the East Anglian coast in the *Europe's Lost Frontiers* study area (Figure 10.2) and measures ~4.3 meters long. Microfossil analysis shows that it contains three depositional settings:

- 0.18-1.34m depth – estuarine mudflats latterly with some algae; initially an eroded peat, with onset of tidal access
- 1.46-4.01m depth – river or lake with some cool/deep water, latterly with hint of low salinity as tidal access approaches with sea-level rise
- 4.27-4.29m depth – till

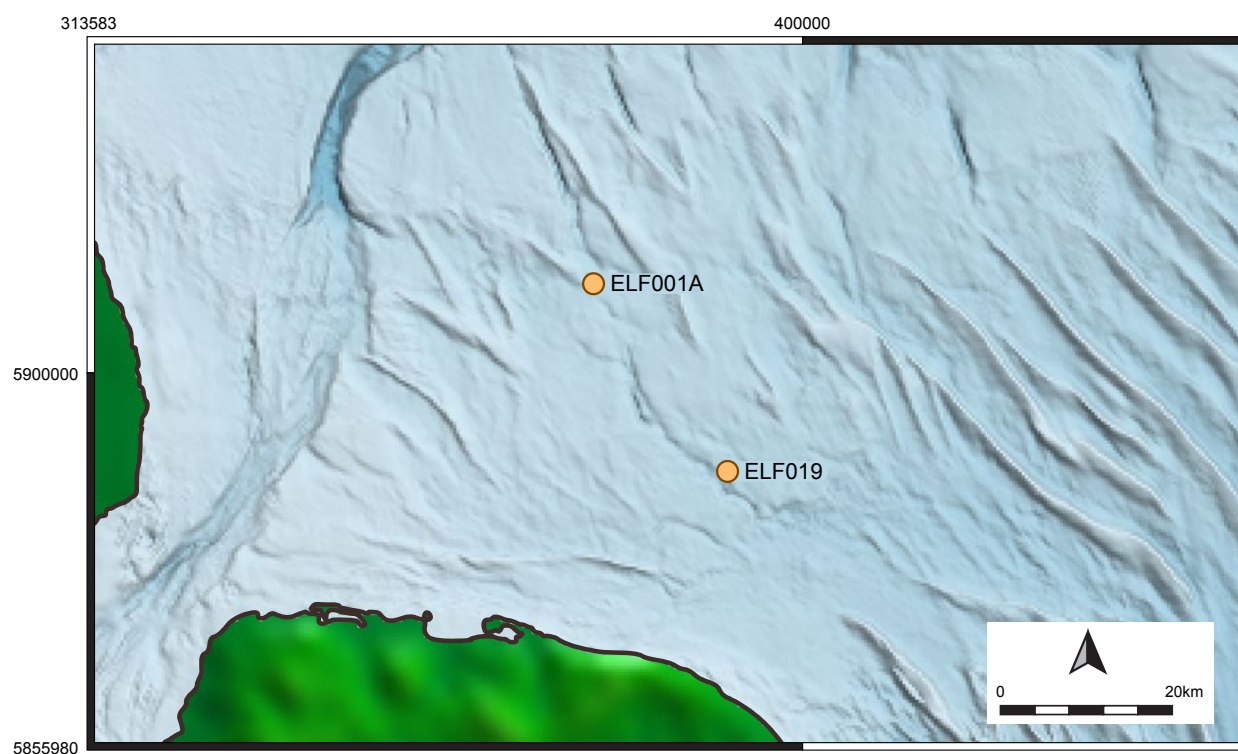


Figure 10.2 Location map of cores referred to in this paper. Bathymetric data is derived from the EMODnet Bathymetry portal - <http://www.emodnet-bathymetry.eu>. Topographic data derived from the NOAA ETOPO1 dataset, courtesy of the NCEI - <https://www.ngdc.noaa.gov/mgg/global/>

The top ~3m of core underwent elemental analysis and the data produced was used for chemostratigraphic interpretation. Chemostratigraphy (chemical stratigraphy) is the application of whole rock or sediment geochemistry to understand the depositional history, correlation and palaeoenvironment of a core. It involves building a chemostratigraphic zonation (chemo zone) of the analysed material, assigning each zone facies information based on its chemistry (chemo facies) and where there is the need, correlating similar chemo zones between different cores and/or outcrops and so producing a chemostratigraphic correlation (Ellwood *et al.* 2008).

The chemo zones produced in ELF19 were driven by variations in detrital grain size, carbonate, clay, organic material and salinity. These variations enabled the core to be subdivided into six chemo zones, each ascribed a chemo facies description. These chemo facies were then compared to available sedimentological and biostratigraphic information to produce a set of integrated core facies.

#### *Elemental data and controls*

Core ELF19 was scanned from a depth of ~18.5cm to ~296cm at a 0.05cm resolution. Reported data underwent the quality control methods outlined above, and eleven elements passed the test (Table 10.1). These elements were subject to PCA analysis (Figures 10.3a

and 10.3b) to establish the dominant mineralogical controls on elemental variation (Table 10.2).

#### *Chemostratigraphic zones*

To establish a chemostratigraphic zonation, the dominant element from each principal component cluster in Table 10.2 were ratioed and plotted for each reported depth down the length of the core. Using ratios to compare elemental data is preferred as this removes any dilution effect caused by variations in other elements analysed at that depth (Weltje *et al.* 2015 and references inter alia). These elemental ratios likely reflect down core variations in:

- Si/Rb: quartz/clay - changes in detrital grain size
- Ca/Rb: carbonate/quartz - marine/fine terrestrial sediment
- S/Rb: organic material/clay
- Br/Ti: salinity (De Boer *et al.* 2014)

Visual comparison of the results of the analysis enabled the core to be split into five chemo zones (numbered top down; Figure 10.4; Table 10.3).

#### *Chemo facies*

It is possible to assign likely chemo facies to the above chemo zones based on their observed chemistry and

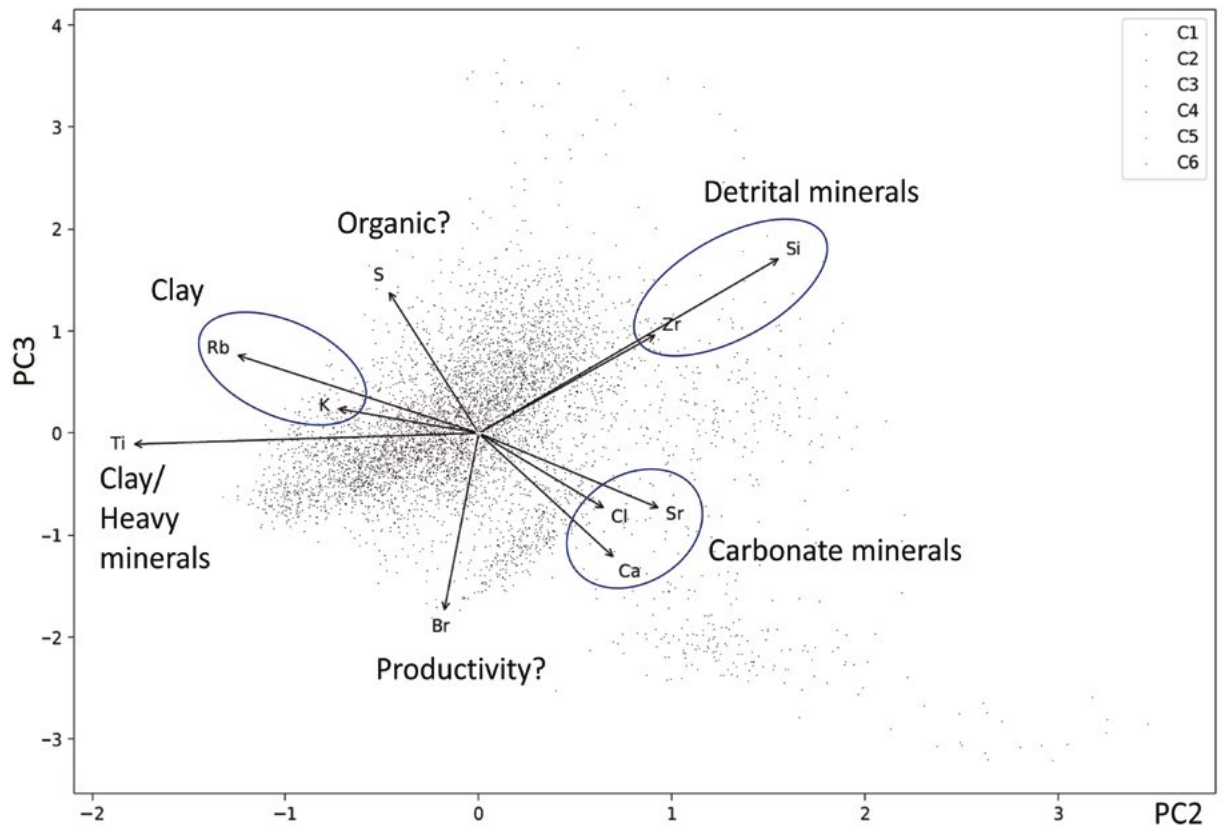
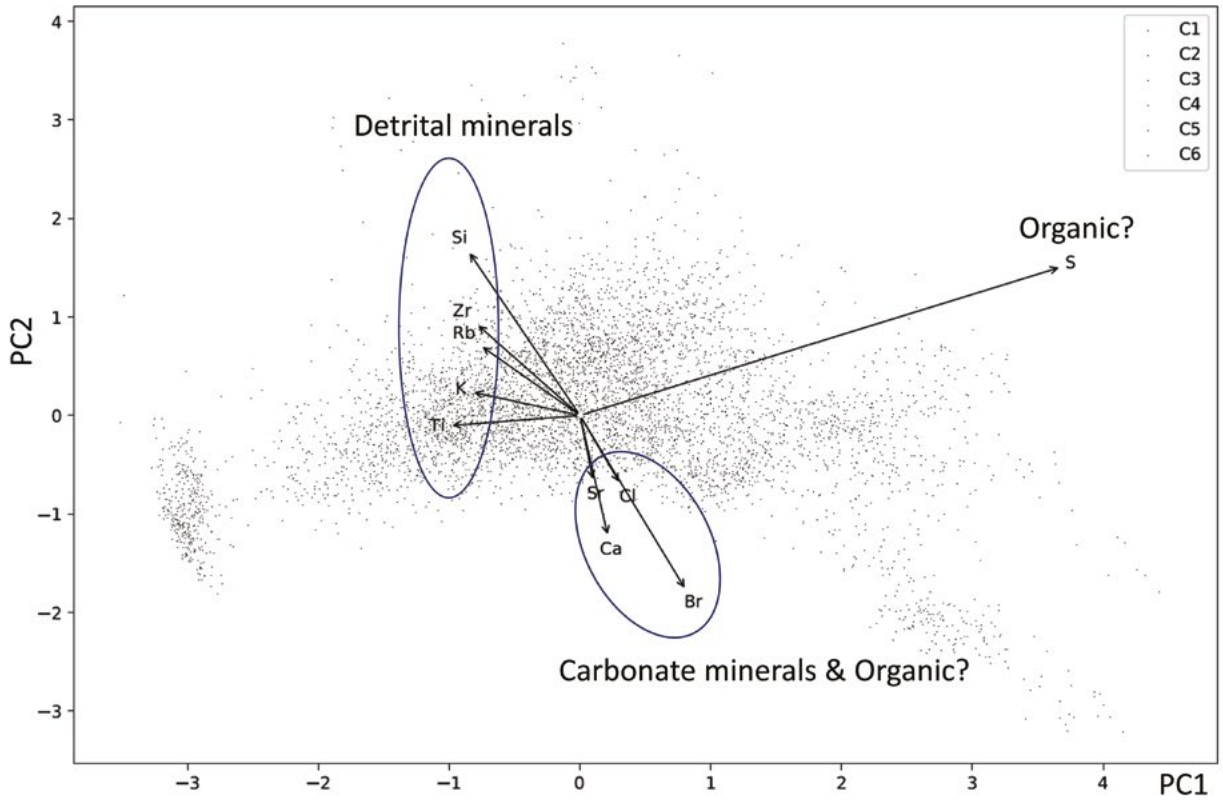


Figure 10.3 PCA of elemental data for core ELF19 showing the likely mineralogical and material drivers for variation in elemental compositions. a - component 1 and 2, b - component 2 and 3.

Element	Symbol	PC1 and 2 control cluster	PC2 and 3 control cluster	Likely mineralogical control
Silicon	Si	Detrital minerals	Detrital minerals	Quartz
Zirconium	Zr			Detrital Zircon
Rubidium	Rb		Clay minerals	Heavy Minerals/Clay minerals/Oxides?
Potassium	K			
Titanium	Ti			
Sulphur	S	Organic material		
Bromine	Br	Carbonate minerals and salinity	Salinity?	Organic material/Salinity?
Calcium	Ca		Carbonate minerals	Carbonate minerals (Calcite)
Strontium	Sr			Carbonate (Aragonite)
Chlorine	Cl			Uncertain - Sea water chemistry?

Table 10.2 Likely elemental affinities for core ELF19.

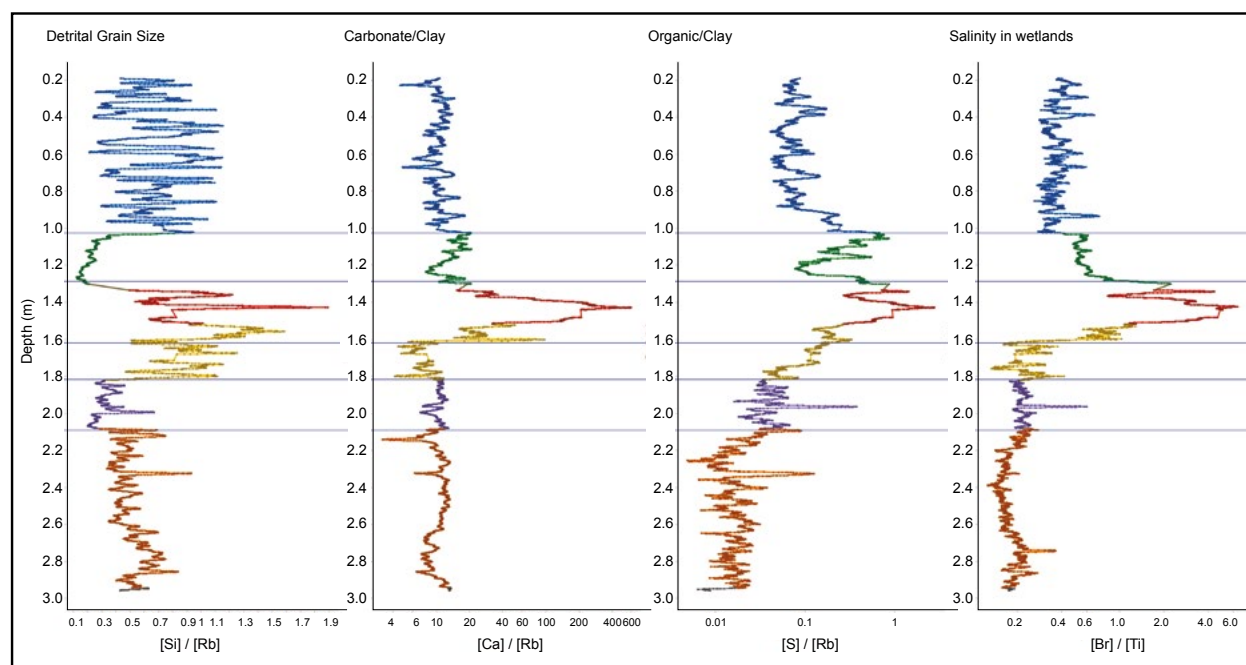


Figure 10.4 Chemostratigraphic zonation of core ELF19. Si/Rb likely reflects variations in grain size with higher values being more Sand (Quartz) rich and higher Rb being more Clay rich. Ca/Rb likely reflects variations in carbonate (Ca) compared to clay material. S/Rb likely reflects variations in organic material (S) to clay. Br/Ti is a proxy for salinity in wetlands (see text for references).

the hypothesised mineralogical controls on chemical data (Table 10.2):

- Chemo zone C1: interbedded sandy/silt and silty/clay horizons (Si/Rb variations) likely of a more saline depositional setting (moderate Br/Ti values) and some shell/carbonate material (Ca/Br); the finer horizons are more organic rich (Si/Rb troughs correlate with S/Rb peaks) and more saline (Si/Rb troughs correlate with Br/Ti peaks)
- Chemo zone C2: massive clay rich unit (very low Si/Rb values) with decreasing downhole organic (S/Rb) content; a higher level of salinity (Br/Ti values)



Chemo Zone	Depth	Si/Rb	Ca/Rb	S/Rb	Br/Ti
		(~Quartz/Clay)	(~Carbonate/Clay)	(~Organic material/Clay)	(~Salinity; (De Boer <i>et al.</i> 2014))
C1		Highly variable, ranging from values of ~1.1 to ~0.01 over ~10cm of stratigraphy	Variable, ranging from ~10 to ~5. Variations occur over a similar scale to Si/Rb and troughs in Ca/Rb correlate with Si/Rb peaks	Moderate (~0.06) with three peaks at ~0.36, 0.6 and 0.7m depth.	Moderate to low
Boundary		Sharp fall	Sharp rise	Sharp rise	Sharp rise
C2		Constantly very low (~0.025)	Moderate to low (~17 at top dropping to ~8 at base of zone)	High at top of unit (0.8) dropping to moderate in centre (~0.08), rising to high again at base (0.5)	Moderate
Boundary		Sharp increase	Sharp increase	Sharp increase	-
C3		Rising to a very high peak in the centre of zone (~1.9)	Rising to a very high peak in the centre of zone (up to ~575)	Rising to a very high peak in the centre of zone (~2.8)	Rising to a very high peak in the centre of zone (~6.4)
Boundary		Trough	Decrease	Decrease	Decrease
C4*		Variable but decreasing from high (~1.6) at top of the zone to moderate at base (~0.8)	Moderate at top of zone (~23) dropping to low at base of zone (~1.7)	Moderate at top of zone (~0.19) dropping to low at base of zone (~0.08)	Moderate at top of zone (~0.8) dropping to low at base of zone (~0.25)
Boundary		Drop	-	Plateauing	Plateauing
C5		Very low/low (0.3)	Low (10.5)	Low (0.04)	Low (0.2)
Boundary		Increase	-	Decrease	Decrease
C6		Moderate (0.5) with a gradual down hole rise.	Low (10.5)	Low (~0.01)	Low (0.2) to very low (0.2) down hole
* Based on the variations in data over the unit it may be possible to split zone C4 into two sub zones.					

Table 10.3 Chemical definition of Chemo Zones and boundaries for core ELF19.

- Ti) than zone C1 some shell/carbonate material (Ca/Br)
- Chemo zone C3: the coarsest unit in the core (Si/Rb) that also contains a large carbonate content (Ca/Rb), organic material (S/Rb) and salinities (Br/Ti)
- Chemo zone C4: a coarse unit (Si/Rb) with low carbonate content (Ca/Rb), decreasing organic material (S/Rb) and low salinity (Ti/Rb)
- Chemo zone C5: a clay rich unit (Si/Rb) with low carbonate content (Ca/Rb), moderate to low organic content (S/Rb) and low salinity (Br/Ti)
- Chemo zone C6: a silty unit (Ca/Rb) with low carbonate content (Ca/Rb), low to very low organic content (S/Rb) and low to very low salinity (Br/Ti)

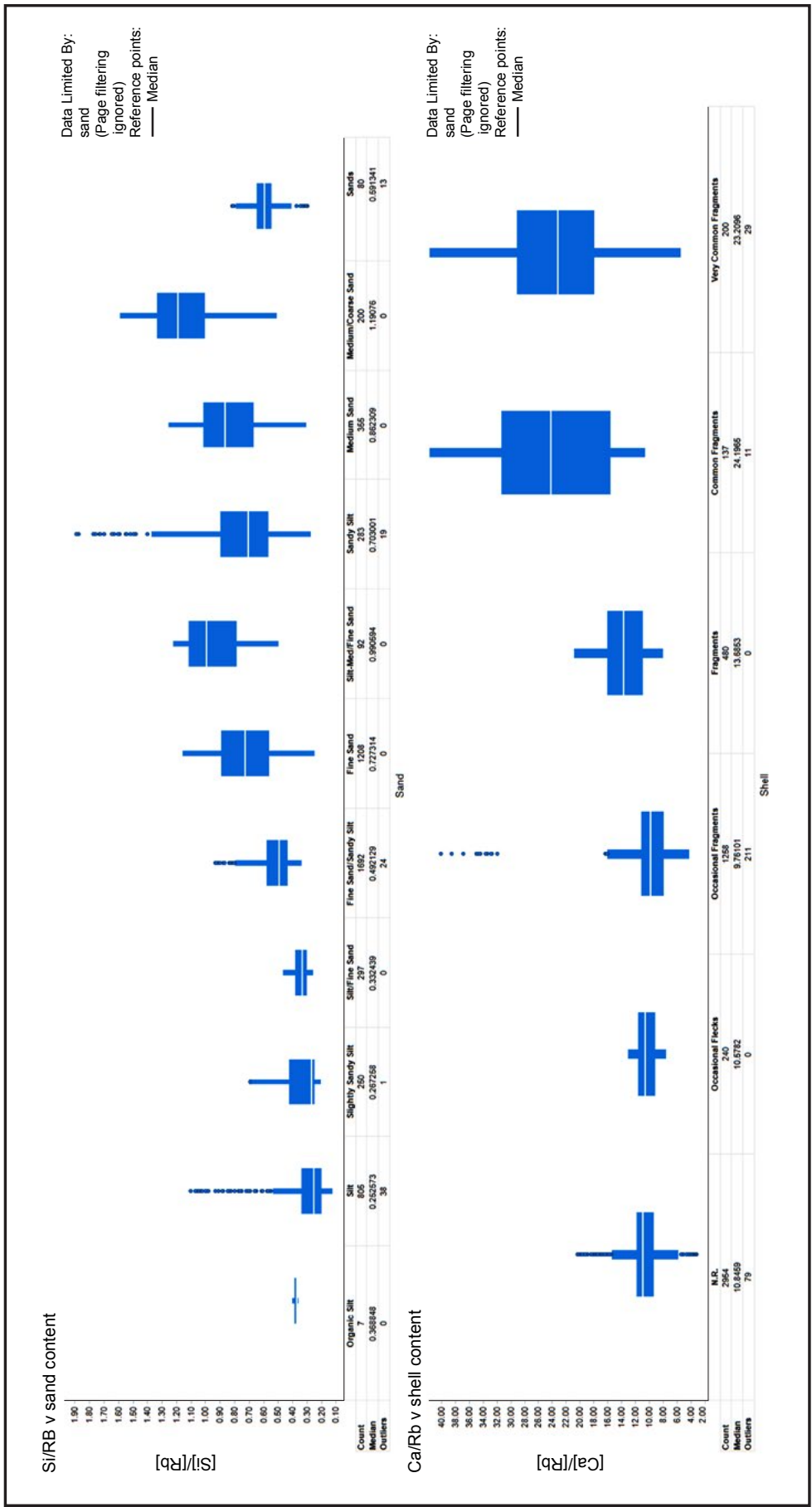


Figure 10.5 Boxplots showing the correlation of observed mineralogy and chemistry within core ELF19.

*Integration of chemo zones with sedimentological and ecological data*

Without any other data the chemo zones presented in section 3.3 are only hypothesised. However, the results can be compared to other geotechnical information such as grain size, shell content and biostratigraphy. A reasonable comparison is achieved between the Si/Rb values and observed sand content as is the comparison of Ca/Rb values with shell contents (Figure 10.5).

When ecological facies, derived from the biostratigraphic data, are compared to chemistry (Figure 10.6) there is also a good coincidence between the ecological boundaries and the chemo zone boundaries. Chemo zones C1 and C2 have Br/Ti values of ~0.4 and S/Rb values of ~0.1 whereas chemo zones C4, C5 and C6 have lower Br/Ti values of ~0.2 and S/Rb values of ~0.05 demonstrating a drop in salinity and organic content down core. Consequently, C1 and C2 are both interpreted as representing estuarine mudflats, whereas, C4-C6 are interpreted as river or lake sediments. Unit C3, shows greater complexity. Based on initial chemistry it is expected this would be a coarse marine bed. The ecological facies data also suggests that this is a coarse unit, however the lack of marine fossils suggest it is deposited in a freshwater setting.

*Conclusions*

The chemostratigraphic zonation of ELF19 based on an interpretation of the chemical, grain size and ecological analysis is summarised in Table 10.4 below.

**Case study 2 – Chemostratigraphic correlation of chemo zones within Holocene shallow cores.**

*Introduction*

Case study 2 seeks to demonstrate how chemostratigraphic zonations can be used to produce a chemostratigraphic correlation for multiple cores across a palaeolandscape for further understanding of palaeotopography, geography and depositional setting.

Chemostratigraphic correlation is a stratigraphic technique that is commonly used in both the petroleum

and minerals industries to correlate core and drill cuttings. This can be undertaken at a variety of different scales from regional scale (Ratcliffe *et al.* 2012), quarry or oil field scale (e.g. Pearce *et al.* 2010) through to field outcrop scale (Ellwood *et al.* 2008). Generally, the more localised the study area the more detailed a correlation is possible.

Chemostratigraphic correlation involves the characterisation, correlation or differentiation of sedimentary rock successions based on stratigraphic variations in the elemental geochemical data. This geochemical data is influenced by changes in the mineralogical and organic content of the rock, and in particular by changes in clay mineralogy and the heavy mineral content. Mineral and organic changes are often a manifestation of changes in palaeoclimate, palaeoenvironment, sediment provenance and both weathering or diagenesis. The dependence of chemostratigraphy techniques on minerals means that it can be used on any lithology, including those that are barren of biostratigraphy. For example, mapping the concentrations of elements such as Zr, Nb and Ti can display changes in heavy mineral abundance, which can provide insight into sediment dispersal patterns and changes in provenance. Mapping elements such as U and Mo reflect the presence and abundance of organic matter that, together with biostratigraphic information, enable the reconstruction of depositional environments.

*Chemostratigraphic correlation*

At the time of writing, work within *Europe’s Lost Frontiers* had not progressed to the point that project data could demonstrate the use of chemostratigraphy to correlate unconsolidated cores, therefore a case study has been produced from data collected from cores sourced from Orkney (Figure 10.7). Three approximately 2 to 3m cores (Core A, B and C), spaced over approximately 300m, were collected from the same sub-basin and underwent geochemical analysis and data interpretation to identify three key elemental ratios:

- Sr/Br – shell material (aragonite)/organic content

Chemo Zone	Top depth (m)	Ecological facies	Integrated interpretation
C1	0.19	Estuarine mudflats	Interbedded estuarine sandy silts and silty clays
C2	1.03	Estuarine mudflats	Estuarine clay
C3	1.33	Freshwater channel in a fluvial system	Coarse sediment of an uncertain marine/fluvial system
C4	1.52	River or lake	Freshwater sands
C5	1.82	River or lake	Freshwater clays with some organic content
C6	2.08	River or lake	Freshwater silts

Table 10.4 Integrated chemical and ecological results for core ELF19.

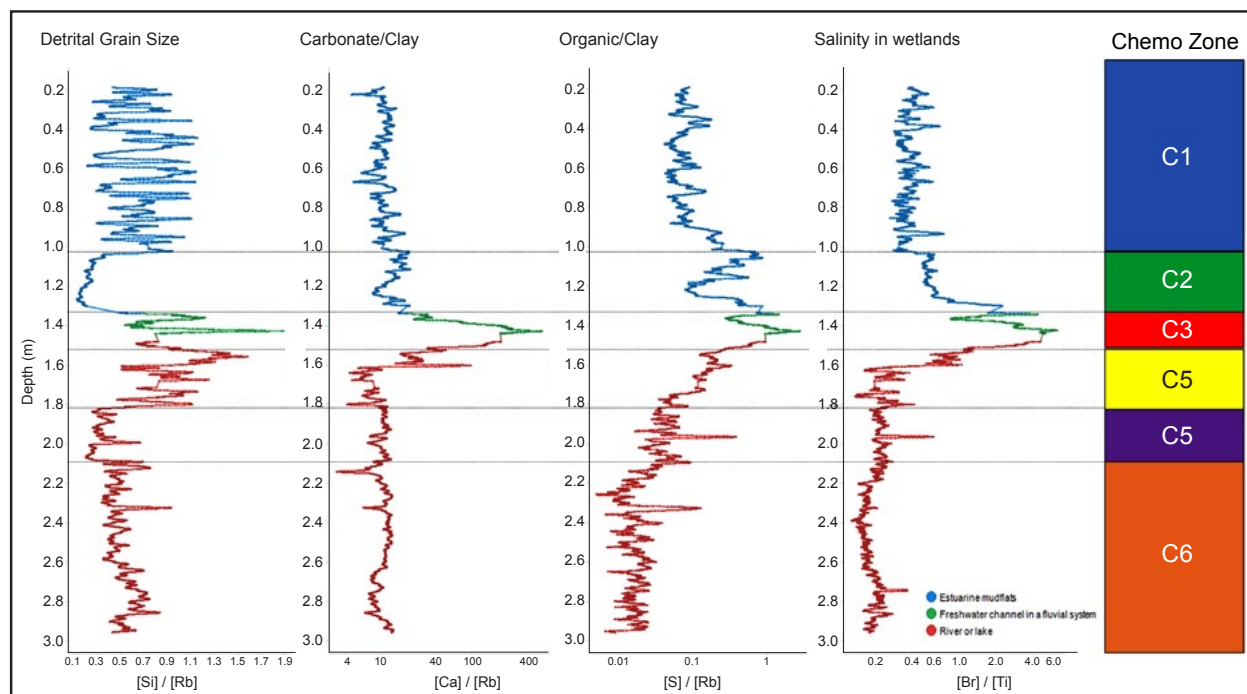


Figure 10.6 This figure demonstrates an excellent match in the chemostratigraphic zonation of core ELF19 and ecological biostratigraphic data.

- Sr/Rb – shell material (aragonite)/clay
- Si/Br – sand (quartz)/organic content

These key ratios were used to establish a chemostratigraphic zonation comprising four chemo zones (C1-C4), furthermore, chemo zone C2 was split into four sub zones (C2-1 to C2-4) in core B and C. Not all zones were present in all cores and so a composite core has been produced to illustrate the full chemostratigraphic zonation (Figure 10.8).

As in case study 1, chemo facies information was produced for each chemo zone. Core B had undergone biostratigraphic analysis and cores A and B had undergone sedimentological analysis and therefore it was possible to 'ground truth' the chemo zonation with other data to produce confident facies descriptions for each chemo zone (Table 10.5).

#### *Chemostratigraphic zonation, correlation and palaeolandscapes interpretation*

The presence and absence of the chemo zones in each core enables the chemo zones and subzones to be correlated across the cores (Figure 10.9 and 10.10).

To the authors knowledge, this represents the first attempt to correlate shallow Holocene cores using chemostratigraphy. Based on this chemostratigraphy, the following depositional history is hypothesised for the study area (further work is currently ongoing to confirm this):

- Chemo zone C1 is found across all three cores, suggesting the carbonate sands blanket the study area
- Chemo zone C2 is only found in cores B and C and thickens from core B to core C; this suggests that this silty unit with differing levels of organic material was either infilling existing topography that deepens towards core C or it has been differentially eroded from the surface – the fact that all subzones within unit C2 thicken towards core C suggest the former is the more likely
- Chemo zone C3 is not found in core B and is underlain by peat in zone C4 – this suggests that core C may have been a sub-aerial peat when the possibly lacustrine C4 sediment was being deposited around it; the lacustrine C3 sediment is also much thicker in core C than A suggesting greater accommodation space formed by palaeotopography
- The peat zone C4 has not been penetrated in core C; in core A it is found below the thin lacustrine C2 unit and so may be present at depth

Due to the high resolution of the scanning XRF, the chemostratigraphic zonation is able to record the exact point at which major palaeoenvironmental changes occurred and the chemostratigraphic correlation map these boundaries spatially (Figure 10.9 and 10.10). Furthermore, the highly precise placement of these palaeoenvironmental changes means that future point sampling (e.g. geochronology, SedaDNA and biostratigraphy) can be carried out at the exact



Figure 10.7 Orkney core locations

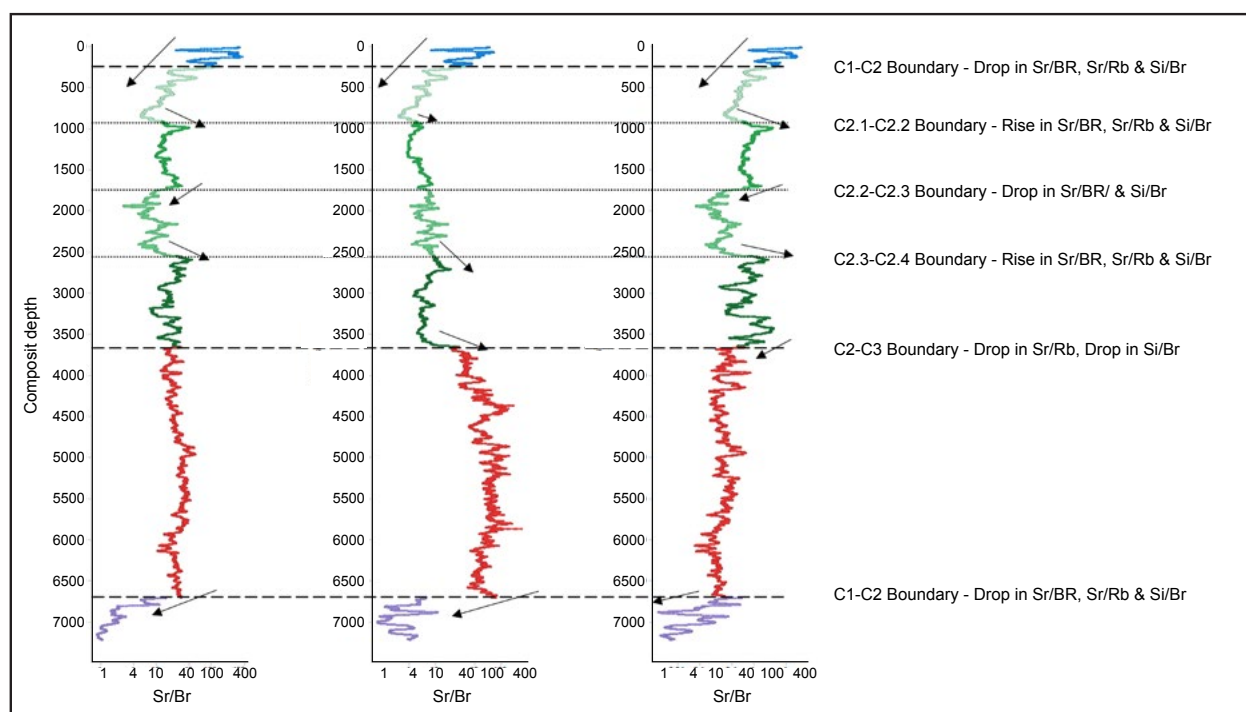


Figure 10.8 The elemental variations utilised to define the chemostratigraphic zonation in the study area. Sr/Br likely reflects variations in shell material (Sr - aragonite) and organic material (Br). Sr/Rb likely reflects variations in shell material (Sr - aragonite) and Clay (Rb). Si/Br likely reflects variations in sand (Si - Quartz) and organic material (Br).

Chemo Zone	Chemical interpretation	Sedimentology	Environmental interpretation	Integrated facies
C1	Shelly sand	Sand, Sand and Mud, Sand and Weed	Freshwater	Shell rich sand
C2	Silt with some shell material. Sub zones C2.1 and C2.3 marked by more organic rich material, where as subzone C2.2 and 2.4 are more shelly and sandy.	Mud	Brackish/ Freshwater	Fresh to brackish silt with some organic rich beds
C3	Carbonate rich	-	Freshwater	Freshwater carbonate rich sediment - Lacustrine?
C4	Low levels of all elements - organic rich sediment?	Peat	-	Peat

Table 10.5 Chemical, sedimentological and environmental interpretation of chemo zones and integrated facies identification.

point these changes take place, removing the need to interpolate between data.

### Case study 3 integrating chemostratigraphy with seismic studies

#### Introduction

This case study seeks to demonstrate how, in addition to producing chemostratigraphic zonation

and correlations from elemental data, incoherent (Compton) and coherent (Rayleigh) scattering caused by the XRF interaction with the core and recorded by the ITrax scanning XRF can be used to calculate a relative density profile for the analysed core. The variations in density can be utilized to link geochemistry to seismic geophysical data and by so doing enable interpretation of palaeo-depositional/environmental scenarios. This can both aid seismic interpretation and be used to extrapolate the chemical analysis away from the core

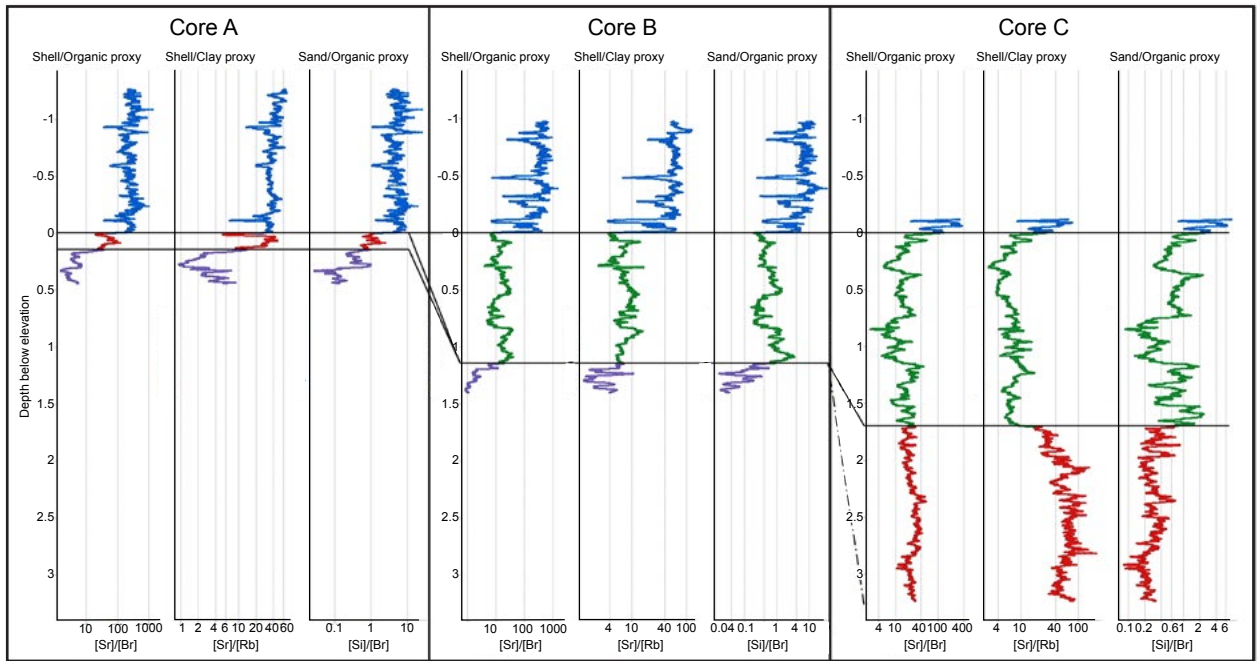


Figure 10.9 Chemostratigraphic correlation of chemo zones in wells A, B and C

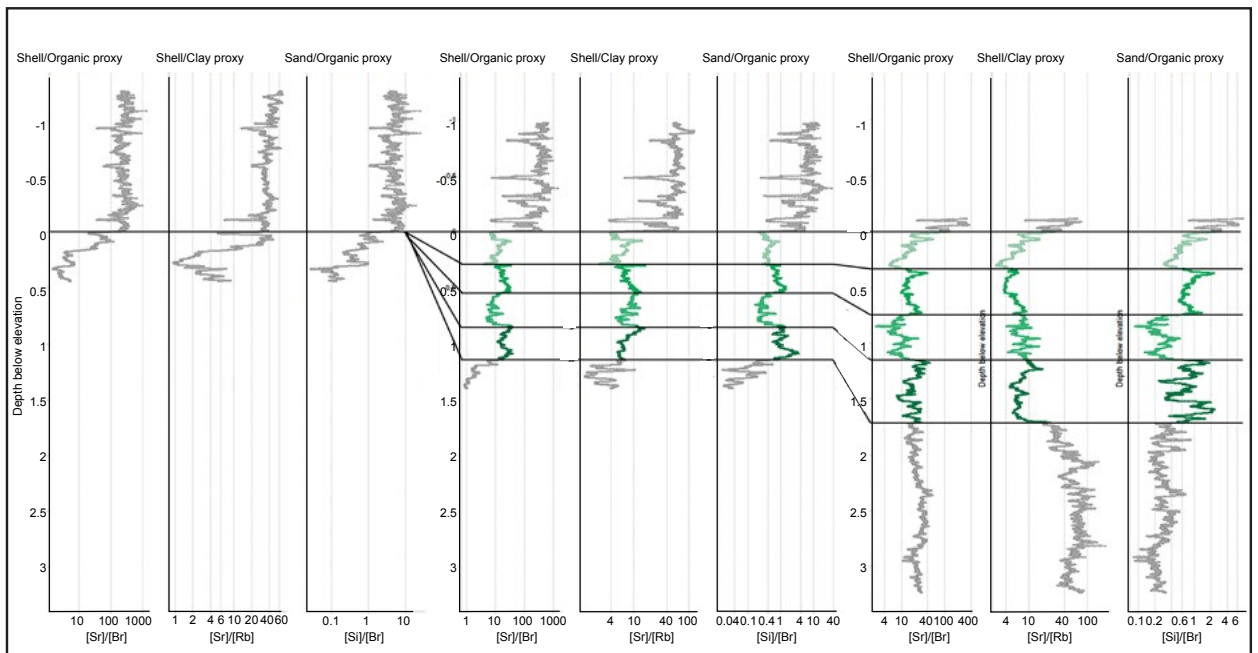


Figure 10.10 Chemostratigraphic correlation of chemo sub zones in wells A, B and C.

locations. This case study utilizes elemental and seismic data published in Gaffney *et al.* (2020) from core ELF1A, which was collected approximately 20 miles north east of core ELF19 (Figure 10.2).

*Chemo zones and facies*

Project core ELF1A has undergone chemostratigraphic zonation with the goal of identifying key geochemical signatures that could result from a tsunami event.

Details of the investigation have been previously presented in Gaffney *et al.* (2020). Using the same method as that outlined in Case study 1, the chemical analysis was used to divide the core into six chemo zones (Figure 10.11) based on variations in:

- Sr – a proxy for shell material
- Rb – a proxy for clay
- Si – a proxy for quartz
- Zr – a proxy for detrital zircon

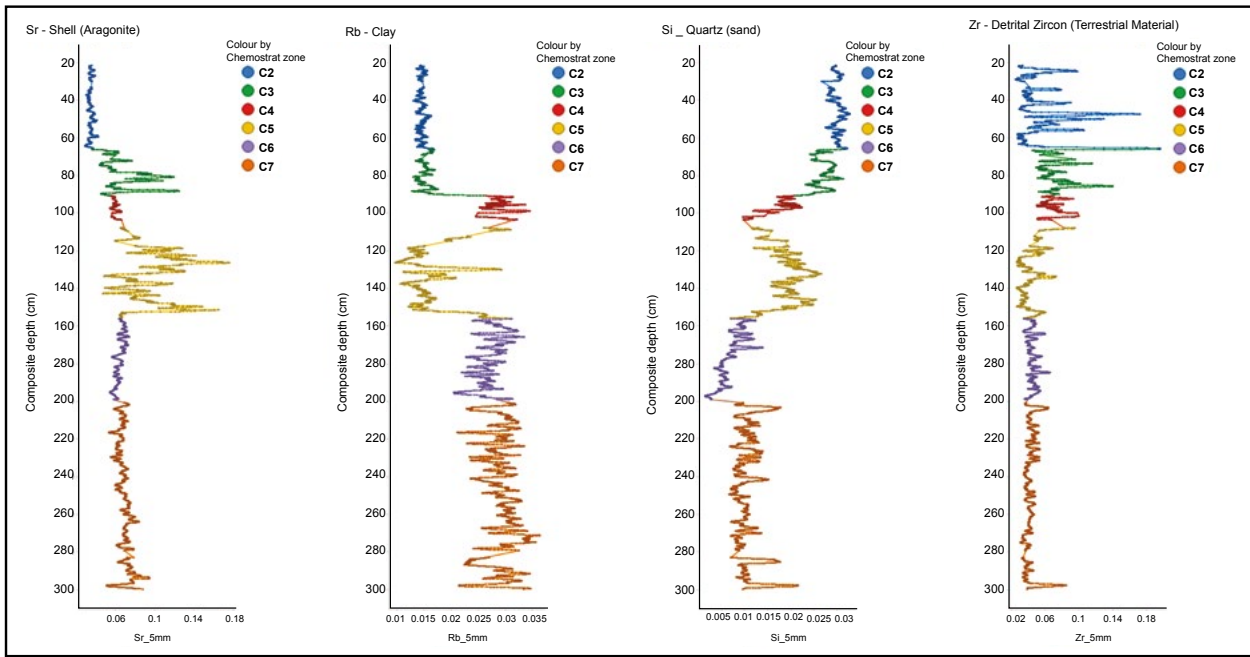


Figure 10.11 Chemostratigraphic zonation of core ELF1A (from Gaffney *et al.* 2020). Sr likely reflects the amount of shell material (aragonite) Rb likely reflects the amount of clay, Si likely reflects the amount of sand (Quartz) and Zr the amount of detrital zircon in the core.

These chemo zones have been interpreted to represent a series of chemostratigraphic facies (Chemo facies) which can be used to understand the depositional environments shown in Table 10.6 (see Gaffney *et al.* 2020 supplementary information).

Chemo zone C5 had been hypothesized to contain a Storegga tsunami deposit, and so a more detailed investigation of this zone was undertaken (Gaffney *et al.* 2020). This enabled the zone to be divided into eight separate sub zones based on changes in:

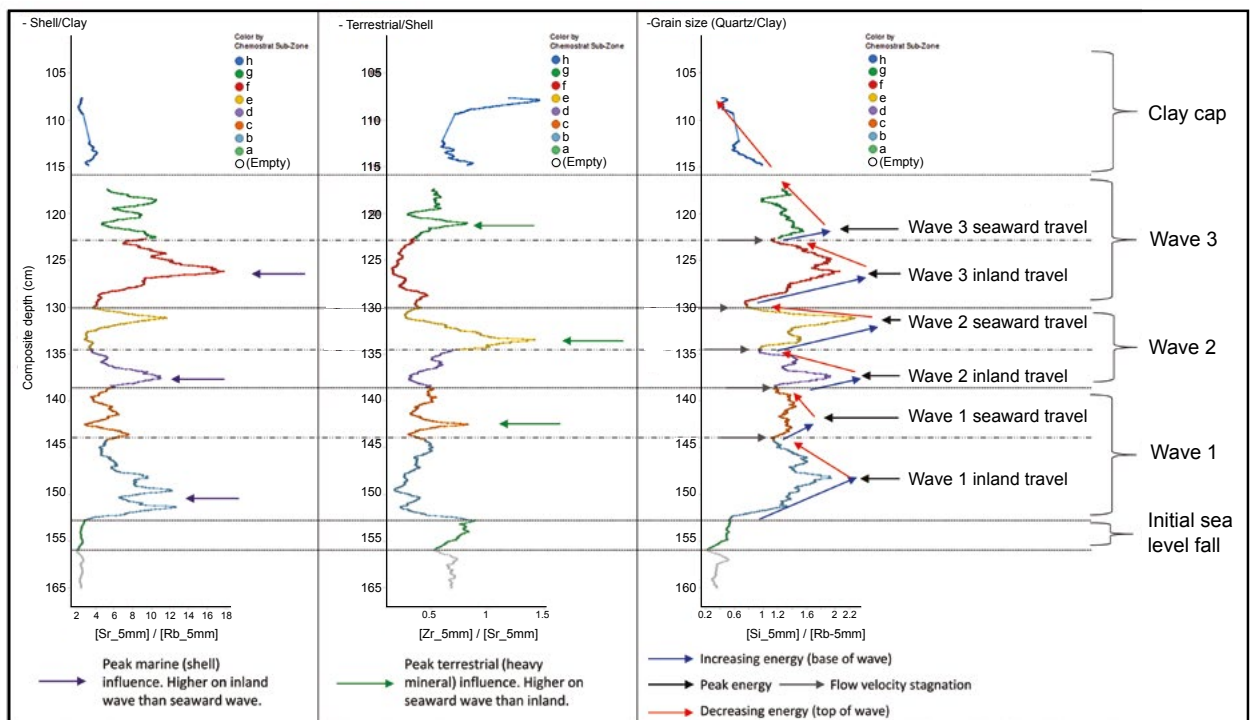


Figure 10.12 Chemostratigraphic zonation of the Storegga tsunami deposit preserved in core ELF1A (from Gaffney *et al.* 2020).



Chemo zone	Chemo facies
C2	A clean high energy sand with little to no shell/marine material or marine influence. Several beds display high Zr/Sr values suggesting increased terrestrial derived heavy mineral sand beds.
C3	A high energy interbedded terrestrial sand and marine/shell dominated deposit.
C4	A clay/silt environment similar to that seen in units C5 and 6 with no shell material, however the moderate Zr/Sr values suggest a more terrestrial input compared to units C5 and 6.
C5	High energy/coarse material including shell/marine material. The large variation in data within C5 does suggest there is an internal stratigraphy (see Gaffney <i>et al.</i> 2020). The top of this unit shows a grading change back to values similar to those in units C6 and 7. These observations suggest this may either be a tsunami or surge deposit; an erosive base, high energy deposit bringing distal marine sediment into a previously terrestrially dominated low energy environment topped by a gradational decrease of energy.
C6	The lowest energy unit in ELF001A is dominated by clay material, little shell material and a constant balanced marine/terrestrial influence.
C7	A clay/silty unit with interbedded siltier horizons (marked by increases in Si/Rb). Little shell material and a constant balanced marine/terrestrial influence.

Table 10.6 Chemo facies identified in core ELF1A (see Gaffney *et al.* 2020 supplementary information for full discussion).

- Sr/Rb – marine signature reflecting the chemical proxy for aragonite as shell content vs clay content
- Zr/Sr – a terrestrial vs marine sediment chemical proxy based on the input of terrestrial detrital zircons compared to a marine shell signal.
- Si/Rb – grain size proxy reflecting the chemical proxy for quartz (coarser sand grain) vs clay content; the coarser-grained sediment indicates a higher depositional energy than the finer clay-sized grains

The eight chemo subzones were interpreted to represent an initial fall in sea level, overlain by deposits associated with three pulses each comprising an initial inland wave identified by its marine depositional signal, topped by a seaward wave characterized by its terrestrial signal (Gaffney *et al.* 2020). The final chemo subzone represented a clay cap, likely reflecting the post tsunami deposition of suspended fine material (Figure 10.12; reproduced from Gaffney *et al.* 2020).

This use of elemental geochemistry enabled the identification of the tsunami deposit which was dated using both C14 and OSL methods. It was postulated that the deposits were associated with the Storegga slide event (Gaffney *et al.* 2020) and represented the furthest south in the North Sea such deposits have thus far been recognised.

### Linking geochemistry to seismic

Several studies have demonstrated that the ratio of the Compton and Rayleigh scattered intensity, recorded by scanning XRF tools, are affected by the average atomic number of the sample, mineralogical composition, water, organic carbon content and therefore density (Fortin *et al.* 2012, Croudace *et al.* 2006). Seismic reflection strength is also a function of the impedance

contrast in velocity, in turn based on elastic moduli, and density, based on lithology/mineralogy, porosity, saturation and organic content of a material. Thus, as the acoustic impedance that produce seismic reflectors are the product of density and velocity so the Compton scattering too is a function of density and there should be a correlation between both.

Core ELF1A has both the interpreted seismic and geochemical data necessary to test this method (see Gaffney *et al.* 2020). There is a large downhole increase in density from approximately 2.6 to 3.2 chemical density units at c. 1.55m depth that corresponds to the base of chemo zone C5 and the tsunami deposit (Gaffney *et al.* 2020). When this is compared to the published seismic (Gaffney *et al.* 2020, Figure 10.12) this is the same depth as the tsunami seismic reflector, suggesting that this method is valid.

Within the XRF data, there are two density changes visible at ~0.8, ~1.15 and ~2m depth. The 0.8 and 1.15m density changes occur at a similar depth to two large amplitude shallow sea floor reflectors in the seismic data (I [green] and II [purple] in Figure 10.13). The ~2m depth density change also coincides with a lower amplitude reflector (IV [black dashed], Figure 10.13). Therefore, we can use the seismic to understand the spatial extent of the chemo zones (Table 10.7). Importantly, this shows how spatially limited the Storegga tsunami deposit is within the study area.

### Future geochemical applications to Europe's Lost Frontiers type studies

This chapter has demonstrated how elemental chemistry can be used to recreate palaeoenvironments within the *Europe's Lost Frontiers* project. It has been shown how geochemistry can be utilised to identify variations in sediment cores (often not visible to the

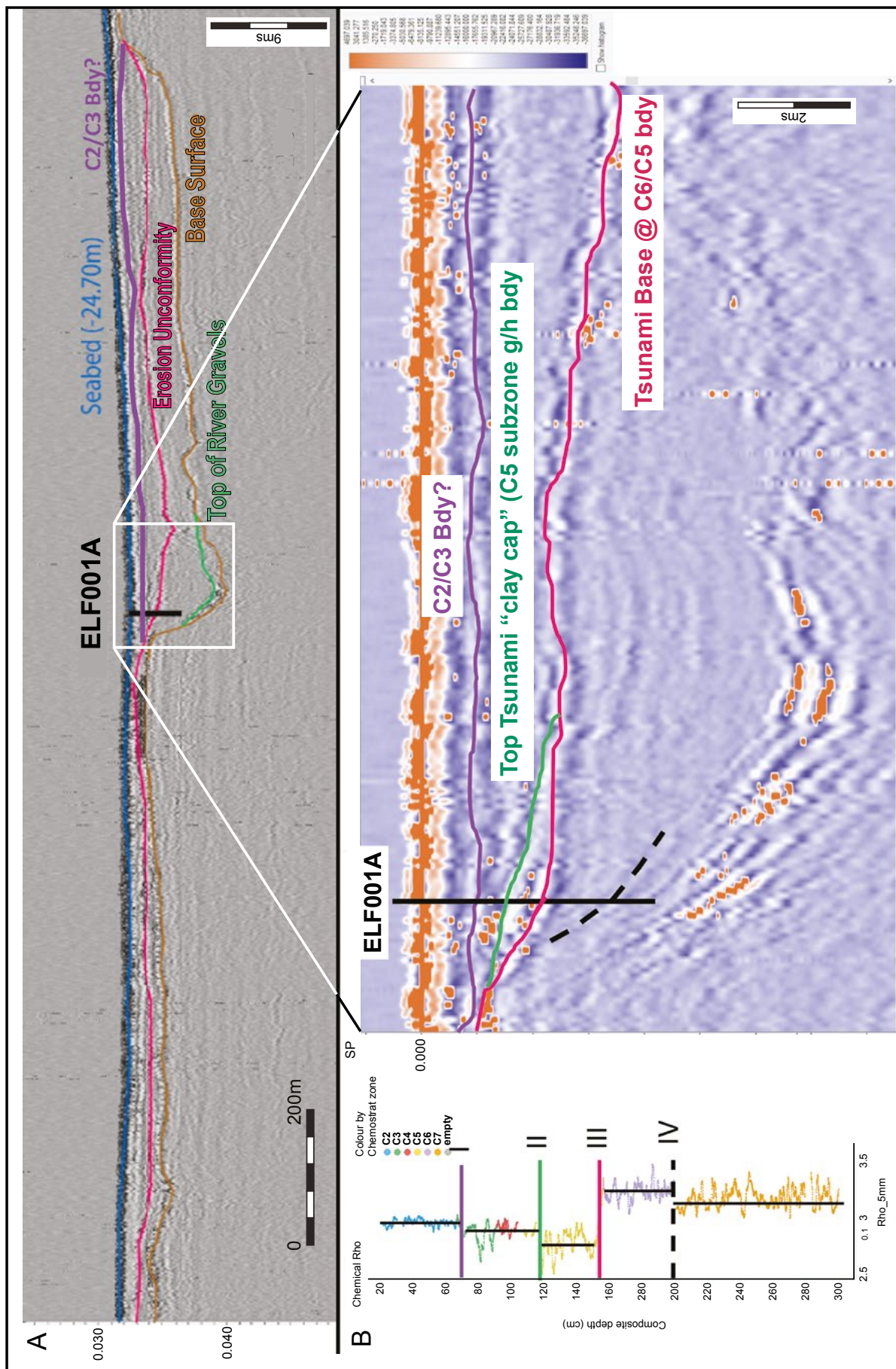


Figure 10.13 Comparison of the relative density of core ELF1A calculated from XRF data to the interpreted seismic data (from Gaffney et al. 2020).

Density change	Chemo zone	Chemo facies variation	Spatial extent on seismic line
I	C2-C3 Bdy	a down hole change from (C2) to sand and shell (C3) material -	laterally continuous
II	Upper C5	The transition between high energy tsunami sediments and the low energy clay cap.	Only found locally to ELF19 - suggests only a small preservation of Tsunami deposit
III	C5-C6 Bdy	Base of Storegga Tsunami deposit	laterally continuous
IV	C6-C7 Bdy	A down hole transition to a clay rich (C7) unit	hard to tell, maybe only local preservation?

Table 10.7 A summary interpretation of geochemical and seismic datasets.

eye) and to chemostratigraphically divide the core into separate chemo zones. It has been shown how the causes of these variations can be understood through statistical methods enabling chemo zones and facies to be assigned and thus in turn aid understanding of the depositional environments. The differentiation and chemostratigraphic correlation of multiple cores has then been undertaken, demonstrating how palaeosurfaces can be identified and palaeolandscapes recreated. There are of additional benefits for conducting geochemical analysis to further the understanding of palaeoenvironments that include:

- with the use of chemical signatures together with stable isotope data to link changes in paleoenvironment with changes in palaeoclimate
- identification of detrital zircon, heavy mineral and chemical provenance signatures in the cores; such studies are commonly utilised in the Carboniferous-Permian hard rock basement, below the Doggerland sediment, identifying if a sediment is sourced from the south (Variscan orogeny/bohemian massif) or north (Norway; e.g, Cram *et al.* 2014) – it is highly probable that this method could be of utility to provenance sand filled channels around Doggerland
- quantitative elemental chemistry is commonly utilised to identify the provenance of clay (e.g. Finlay *et al.* 2012) and geological materials (e.g. Bevins *et al.* 2020) in archaeological studies – could these methods be applied to lithic materials dredged from Doggerland and so both establish chemical families of lithics and potentially even correlate them to known (Present day) onshore sites?

- the chemo zones presented in this study are all linked to natural changes in the sediment record – however, could some of them be signals of human activities such as habitation? For example:
  - within North Sea oil and gas studies, the Si/Zr ratio is commonly utilised to identify flints in chalks – could this ratio be used to identify micro-debitage from knapping sites?
  - phosphorus is commonly associated with coprolite and hardgrounds – could it be used to identify phosphates caused by animal and human waste, vivianite or bone beds?
  - can Sr data be utilised to identify shell middens?

Elemental geochemistry is a powerful tool for archaeological and palaeoenvironmental studies. It can be used to identify depositional changes in any fluvial, lacustrine, marine or terrestrial setting, and correlate them across study areas, revealing palaeo- surfaces and landscapes. The wide range of modern analytical tools, from portable closed source tools that can be deployed in the field, through to lab-based scanning XRF tools that are capable of recording high vertical resolution data mean that geochemistry is a highly flexible tool suitable for application to a wide variety of settings. Furthermore, the ability to use geochemical tools to generate density data means that the results are easily linked to other investigative techniques, such as geophysics, and so aid the integration of disparate analytical datasets. Therefore, it is hoped that elemental geochemistry will become an increasingly utilised tool for studies across archaeology, palaeoenvironmental sciences and the humanities.